FEMS Microbiology Ecology, 2024, **100**, fiae103
DOI: 10.1093/femsec/fiae103
Advance access publication date: 22 July 2024
Research Article

Microbial remineralization processes during postspring-bloom with excess phosphate available in the northern Baltic Sea

Mari Vanharanta [1,2,*], Mariano Santoro [3,4], Cristian Villena-Alemany [5], Jonna Piiparinen [2], Kasia Piwosz [6], Hans-Peter Grossart [7,8], Matthias Labrenz [3], Kristian Spilling [2,9]

[1]Tvärminne Zoological Station, University of Helsinki, J. A. Palménin tie 260, 10900 Hanko, Finland
[2]Marine and Freshwater Solutions, Finnish Environment Institute, Latokartanonkaari 11, 00790 Helsinki, Finland
[3]Department of Biological Oceanography, Leibniz Institute for Baltic Sea Research Warnemünde - IOW, Seestrasse 15, 18119 Rostock, Germany
[4]Department of Plant Physiology, Institute for Biosciences, University of Rostock, Albert-Einstein-Str. 3, 18059 Rostock, Germany
[5]Laboratory of Anoxygenic Phototrophs, Institute of Microbiology, Czech Academy of Sciences, Novohradská 237 - Opatovický mlýn, 379 01 Třeboň, Czech Republic
[6]Department of Fisheries Oceanography and Marine Ecology, National Marine Fisheries Research Institute, ul. Kołłątaja 1, 81-332 Gdynia, Poland
[7]Department of Plankton and Microbial Ecology, Leibniz Institute for Freshwater Ecology and Inland Fisheries, Alte Fischerhütte 2, OT Neuglobsow, 16775 Stechlin, Germany
[8]Institute of Biology and Biochemistry, Potsdam University, Maulbeerallee 2, 14469 Potsdam, Germany
[9]Centre for Coastal Research, University of Agder, Universitetsveien 25, 4604 Kristiansand, Norway
*Corresponding author. Tvärminne Zoological Station, University of Helsinki, J. A. Palménin tie 260, 10900 Hanko, Finland. E-mail: mari.vanharanta@syke.fi
Editor: [Veljo Kisand]

Abstract

The phosphorus (P) concentration is increasing in parts of the Baltic Sea following the spring bloom. The fate of this excess P-pool is an open question, and here we investigate the role of microbial degradation processes in the excess P assimilation phase. During a 17-day-long mesocosm experiment in the southwest Finnish archipelago, we examined nitrogen, phosphorus, and carbon acquiring extracellular enzyme activities in three size fractions (<0.2, 0.2–3, and >3 µm), bacterial abundance, production, community composition, and its predicted metabolic functions. The mesocosms received carbon (C) and nitrogen (N) amendments individually and in combination (NC) to distinguish between heterotrophic and autotrophic processes. Alkaline phosphatase activity occurred mainly in the dissolved form and likely contributed to the excess phosphate conditions together with grazing. At the beginning of the experiment, peptidolytic and glycolytic enzymes were mostly produced by free-living bacteria. However, by the end of the experiment, the NC-treatment induced a shift in peptidolytic and glycolytic activities and degradation of phosphomonoesters toward the particle-associated fraction, likely as a consequence of higher substrate availability. This would potentially promote retention of nutrients in the surface as opposed to sedimentation, but direct sedimentation measurements are needed to verify this hypothesis.

Keywords: excess phosphate; extracellular enzyme activity; mesocosm; northern Baltic Sea; organic matter degradation; postspring-bloom

Introduction

The diatom and/or dinoflagellate-dominated spring bloom in the Baltic Sea ends upon the depletion of dissolved inorganic nitrogen (DIN) and, in large parts of the Baltic, typically an excess phosphate concentration of >0.2 µmol l^{-1} remains in the upper water layer (Spilling et al. 2018). This condition is regarded to induce recurring summer blooms of N_2-fixing cyanobacteria (Niemi 1979, Rahm et al. 2000, Vahtera et al. 2007, Lilover and Stips 2008). However, the main period of cyanobacterial blooms usually starts 2–3 months after the termination of the spring bloom, when the excess phosphate has already been consumed by other organisms (Raateoja et al. 2011, Lips and Lips 2017, Vanharanta and Spilling 2023).

The typical postspring-bloom low dissolved inorganic nitrogen to phosphorus ratio (DIN:DIP ~2) indicates strong N-limitation of planktonic productivity (Lignell et al. 2008). This condition likely enhances remineralization of organic nitrogen-rich compounds (Eilola and Stigebrandt 1999) that could allow for the utilization of the excess phosphate pool. The low DIN:DIP ratio may favor the growth of heterotrophic bacteria that have generally low DIN:DIP uptake ratio and high affinity to phosphate due to a relatively low C:P of 45 in their biomass (Kirchman 1994, Nausch et al. 2018). Effective uptake of DIP together with organic forms of nitrogen has the potential to turn the system into combined N and P deficiency (Lignell et al. 2008), but heterotrophic bacteria might be limited by labile carbon-rich substrates (Kirchman 1994, Lignell et al. 2008).

Biological remineralization processes are driven by microbially synthetized extracellular enzymes, which hydrolyze high molecular weight organic matter (OM) into smaller substances, thus enabling the acquisition of organic monomers and mineral nutrients into microbial cells. These enzymes exist either attached to their producing cell (i.e. cell-attached) in which case the hydrolysis products are near the cell surface for transport and

Received 7 February 2024; **revised** 10 June 2024; **accepted** 19 July 2024

subsequent intracellular metabolism, or secreted into the water (i.e. dissolved) when hydrolysis products are available also for the nonenzyme producing organisms. Depending on the circumstances, either of these forms of OM hydrolysis can be optimal (Traving et al. 2015), and different phyla of heterotrophic bacteria possess varying strategies of enzyme production (Murray et al. 2007, Allison et al. 2014, Ramin and Allison 2019). Different forms of substrate hydrolysis can also depend on the phytoplankton bloom type (Grossart et al. 2007a) or phase and environmental conditions, and this can be either due to community change or ability of individual cells to shift between substrate hydrolysis strategies (Traving et al. 2022) that could be related to their ability to alternate between free-living and surface-attached stages (Grossart 2010).

Dissolved enzymes can originate from direct release by prokaryotes attached to particles or colloids in low diffusion and high substrate environments (Ziervogel and Arnosti 2008, Baltar et al. 2010, Ziervogel et al. 2010), bacterial stress and mortality (Baltar et al. 2019), cell lysis due to viral infection (Karner and Rassoulzadegan 1995) and protist grazing on bacteria (Bochdansky et al. 1995). Also, fungi (Grossart et al. 2019, Salazar-Alekseyeva et al. 2023) and autotrophs such as diatoms (e.g. Rengefors et al. 2001) and mixotrophic algae (Salerno and Stoecker 2009) produce extracellular enzymes that, e.g. during phytoplankton bloom breakdown can end up in the dissolved enzyme pool. In the Baltic Sea, alkaline phosphatase (APase) activity has been attributed to phytoplankton (Nausch 1998) and is often found in the cell-attached form (González-Gil et al. 1998, Strojsová et al. 2003), whereas up to 30% of the bacterial APase activity appears to be dissolved (Luo et al. 2009). The ecologically significant characteristic of dissolved enzymes is that they may remain functional in the water column for days to weeks after being released into the surrounding water (Hoppe 1991, Ziervogel et al. 2010, Steen and Arnosti 2011, Thomson et al. 2019). Thereby, they spatially and temporally decouple hydrolysis products and enzyme producing cell (Ziervogel et al. 2010, Baltar 2018).

In a recent indoor tank experiment, a larger part of the excess phosphate remaining after the spring bloom ended up in the particulate organic phosphorus (POP) pool than in the dissolved organic fraction (Vanharanta and Spilling 2023), which would imply OM flux to the seafloor and sedimentation of the excess phosphate. However, the particulate form might be heavily colonized by bacteria (Bochdansky et al. 2016), which could potentially enhance OM remineralization and nutrient cycling in the upper water layer microbial food web (Malfatti et al. 2014). The magnitude of vertically transported OM depends on several other factors as well, including packaging, size spectrum, and chemical composition of the particles (Cho and Azam 1988).

As part of a larger study on the fate of excess phosphate in the northern Baltic Sea, the present paper reports the enzymatic processing of OM under low DIN:DIP ratio relative to the canonical N:P Redfield ratio 16:1 (Redfield 1958). Inorganic nutrient supply and availability of labile carbon sources influence the uptake stoichiometry and resource competition between primary producers and heterotrophic bacteria with consequences for further trophic interactions (Thingstad et al. 2008). The development of the plankton community during this experiment is presented in Spilling et al. (2024). The main aim of this study was to investigate the possible drivers of EEAs and the degradation potential of organic material that determines the availability of regenerated nutrients for maintaining autotrophic growth and ultimately affects the potential of OM export to the sea floor after the northern Baltic spring bloom. In addition, we described the bacterial community composition and compared the measured EEAs with the predicted functional abundances of the bacterial taxa identified via 16S rRNA gene sequences. We hypothesized that (1) DIN limitation and excess phosphate availability enhance the degradation of dissolved organic nitrogen (DON) enabling the assimilation and probable subsequent sedimentation of the excess phosphate pool and consequently could drive the system into codeficiency of DIN and DIP and that (2) heterotrophic bacteria may be also limited by labile carbon substrates, which reduces their competitive edge against picophytoplankton for inorganic nutrients.

Materials and methods

Experimental design and sampling

An outdoor mesocosm experiment was conducted between 7th and 23rd June 2021. Scientific foundation and details of the experimental setup are given in Spilling et al. (2024). Briefly, we moored 14 transparent plastic mesocosm bags (volume 1.2 m^3, diameter 0.9 m, and depth 2 m) in a linear array beside a pontoon off Tvärminne Zoological Station at the Finnish southwest coast (59°50′37″N, 23°15′6″E). Mesocosms were filled with surface water by gentle pumping with a submersible pump (Junhe Pumps Holding CO, LTD) on 7th June marking day −1 of the experiment. Microscopy sample indicated that this pumping method did not affect zooplankton but prevented small fish from entering the mesocosms (Spilling et al. 2024). Temperature (∼18°C) and salinity (5.5 psu) were measured using a portable calibrated digital water meter (MU 6100 H, VWR). Dummy bags filled at each end ensured the same light conditions in mesocosm 1 and 12. All mesocosms were partially protected from rain and bird feces with a transparent plastic roof.

On experiment day 0 (8th June), the concentration of DIP was 0.013 µmol l^{-1} and each of the 12 mesocosms received an addition of PO_4^{3-} (KH_2PO_4) to a starting concentration of 0.66 µmol l^{-1} to simulate the excessive DIP conditions prevailing in the Gulf of Finland after the spring bloom. In addition to three otherwise unamended control mesocosms, the experimental design consisted of three different triplicate treatments: carbon addition as glucose (C-treatment), nitrate addition (N-treatment), and combined carbon and nitrate additions (NC-treatment). Before the start of the experiment there was 0.031 µmol DIN l^{-1} in the water. Nitrate (NO_3^-) was added in each of the three N- and NC-treated mesocosms to a final starting concentration of 3.66 µmol NO_3^- l^{-1}. The resulting DIN:DIP ratio in the N-amended mesocosms was ∼5.5. Glucose was added to each of the three C- and NC-treated mesocosms to final concentration of 36 µmol C l^{-1}. All additions were made on day 0, right before the first full sampling.

Water samples for extracellular enzyme activities, chlorophyll-*a*, inorganic nutrient, particulate, and dissolved organic nutrient concentrations, bacterial abundance, and thymidine and leucine incorporation-based bacterial production (BPT and BPL, respectively), as well as DNA extraction for 16S rRNA analysis and abundance of heterotrophic nanoflagellates were taken on days 0, 1, 3, 6, 8, 10, 13, and 15 with a Limnos sampler (Hydro-Bios, Germany) at a depth of 0.5 m. Temperature was measured inside the mesocosms by logging sensors (HOBO U26; Onset Inc, US) throughout the entire experiment. Water collected from each mesocosm was transported in acid-washed and MQ-rinsed closed 5 l plastic containers, previously prerinsed with the sampled water, to a climate chamber in the laboratory for further processing.

Chemical analyses

Dissolved inorganic nutrients (NO_3^-+NO_2^-, PO_4^{3-}) were measured by standard colorimetric methods (Grasshoff et al. 1999) using a photometric analyzer (Thermo Scientific Aquacem 250). NH_4^+ was measured with a Hitachi U-1100 spectrophotometer.

Chlorophyll-*a* concentration was determined according to Jespersen and Christoffersen (1987) by filtering 50 ml of sample in duplicates onto GF/F filters (pore size 0.7 µm, Whatman) and extracted with 94% ethanol in the dark at room temperature for 24 h before analysis with a fluorometer (Varian Inc., Cary Eclipse). Chlorophyll-*a* measurements were calibrated with a chlorophyll-*a* standard (Sigma).

Samples for dissolved organic carbon (DOC) and total dissolved nitrogen (TDN) (20 ml) were filtered into acid-washed and precombusted glass vials through 0.2 µm polycarbonate syringe filters (Whatman, UK). Samples were acidified with 2 M HCl and concentrations were determined by high-temperature catalytic oxidation according to Sharp et al. (1993) using a Shimadzu TOC-VCPH carbon and nitrogen analyzer equipped with a chemiluminescence detector (Shimadzu TNM-1) for measuring TDN. DON was calculated as the difference between TDN and DIN. Total dissolved phosphorus (TDP) concentration was determined according to Koistinen et al. (2017) from 30 ml of sample water filtered through 0.2 µm polycarbonate syringe filters (Whatman) into acid-washed centrifuge tubes. Dissolved organic phosphorus (DOP) was calculated as the difference between TDP and DIP.

For determination of particulate organic nutrient concentrations, 100 ml of water was filtered in duplicates onto acid-washed (2 M HCl for 15 min), rinsed with ultrapure water, and precombusted (450°C, 4 h) GF/F filters (Whatman). Concentrations of particulate organic carbon (POC) and nitrogen (PON) were measured with a CHN element analyzer coupled to a mass spectrometer (Europa Scientific ANCA-MS 20–2015 N/13C) (Salonen 1979). Concentration of particulate organic phosphorus (POP) was measured by dry incineration and acid hydrolysis (Solórzano and Sharp 1980) with modification by Koistinen et al. (2017). Particulate organic elemental ratios POC:PON:POP were calculated on a molar basis.

Biovolume estimates

The microphytoplankton composition and total biovolume were determined using FlowCam (see further methodological details in Spilling et al. 2024), which detects particles within the size range of 2–100 µm. The contribution of detritus to the total biovolume was used as an indicator of OM quality.

Bacteria abundance and bacterial production

Heterotrophic bacteria were enumerated by flow cytometry (LSR II, BD Biosciences, USA) using a 488-nm laser. Samples were fixed with 1% paraformaldehyde (final concentration) for 15 min in darkness, flash frozen in liquid nitrogen, and stored at −80°C until analysis. Prior to flow cytometry, samples were stained with SYBR-Green I (Molecular Probes, Eugene, OR, USA) at a 10^{-4} (v/v) concentration and incubated for 15 min in the dark according to Gasol and Del Giorgio (2000). CountBright beads (Molecular Probes) were added to each sample to determine measured volume. Heterotrophic bacteria were detected according to their green fluorescence and side scatter properties using the FACSDiva Software (BD Biosciences). Cell counts were obtained with the Flowing Software version number 2.5.1 (https://bioscience.fi/?s=flowing+software).

Bacterial production (µmol C l^{-1} h^{-1}) was measured as incorporation of ^{3}H-thymidine (BPT) and ^{14}C-leucine (BPL) using cold trichloroacetic (TCA) extraction (Fuhrman and Azam 1982, Kirchman et al. 1985). Of each sample three replicates and two formaldehyde-fixed (final concentration 1.85%) adsorption blanks were spiked with [methyl-^{3}H]-thymidine and L-[^{14}C(U)]-leucine (Perkin Elmer) at saturating concentrations of 20 nM and 150 nM, respectively. The subsamples (1 ml) were incubated in Eppendorf tubes for 1–1.5 h in the dark at ∼17°C and the incubation was stopped by addition of formaldehyde (final concentration of 1.85%). TCA extraction was done using the centrifugation method (Smith and Azam 1992) after which the pellets were dissolved in Instagel scintillation cocktail for measurements with a Wallac Win Spectral 1414 liquid scintillation counter. A cell conversion factor of 1.4 × 10^9 cells $nmol^{-1}$ (HELCOM 2008) and a carbon conversion factor of 0.12 pg C × (μm^3 $cell^{-1}$)$^{0.7}$ (Norland 1993) were used to convert thymidine incorporation to carbon production. Based on earlier measurements an average bacterial cell volume of 0.06 μm^3 was used (Hoikkala, personal communication). Leucine incorporation was converted to carbon production using a factor of 1.5 kg C mol^{-1} (Simon and Azam 1989).

Heterotrophic nanoflagellates

Abundance of aplastidic nanoflagellates (cell size <20 µm) was estimated using epifluorescence microscopy. A volume of 20 ml of sample was filtered onto white polycarbonate filters (diameter 25 mm, pore size 0.8 µm). The cells were stained with 4′,6-diamidino-2-phenylindole solution (concentration 1 µg ml^{-1}) for 10 min in the dark and manually counted using Leica M125 with integrated camera and fluorescence capability (Germany) according to Sherr et al. (1987).

Extracellular enzyme activities

Hydrolytic rates of four enzymes; APase, β-glucosidase (BGase), α-glucosidase (AGase), and leucine aminopeptidase (LAPase) were measured as an increase in fluorescence over a 4-h incubation in the dark at ∼17°C. Fluorescence was measured in 1 h intervals with an Agilent Cary Eclipse Fluorescence Spectrophotometer with excitation/emission wavelengths of 360/450 nm on Nunc 96-well plates (sample volume 330 µl). Working solutions of fluorogenic model substrate analogs corresponding to classes of natural substrate chemical bonds, 4-methylumbelliferyl-phosphate (APase), 4-methylumbelliferyl-βD-glucopyranoside (BGase), 4-methylumbelliferyl-αD-glucopyranoside (AGase), and L-leucine-7-amido-4-methylcoumarin (LAPase) (Sigma, Aldrich) were prepared according to Hoppe (1983) and added in samples at previously tested saturating final concentrations of 100 µM (APase, BGase, and AGase) and 500 µM (LAPase). Consequently, measured hydrolytic rates represent potential values proportional to the pool of extracellular enzymes present in the sample (Hoppe 1983). Substrate analogs were measured in four replicates per sample. Fluorescence was converted to microbial enzymatic activity (nmol l^{-1} h^{-1}) by standard curves established with a range of increasing concentrations of chromophores 4-methylumbelliferone and 7-amido-4-methylcoumarin added in 0.2 µm filtered sample water according to Baltar et al. (2016). Autoclaved water samples as controls have previously indicated negligible background activity.

Sample water for EEA measurements was size fractionated by filtering a subsample through sterile 0.2 µm low protein binding Acrodisc filters (Pall) and another subsample through 3 µm Nuclepore Track-Etch Membrane filters (Whatman). The <0.2 µm fraction is assumed to contain free dissolved enzymes. The EEA in size fraction 0.2–3 µm was obtained from the difference in activities in 0.2 and 3 µm filtrates and mainly represents extracellular enzymes attached to free-living bacteria or dissolved enzymes

attached to small abiotic surfaces. In addition, activity in unfiltered sample water was measured for obtaining the >3 µm activity by calculating the difference in activities in the nonsize fractionated sample water and the <3 µm filtrate. This fraction represents either particle-attached microbes, dissolved enzymes absorbed to abiotic particles, or enzymes produced by large phytoplankton cells. Bacteria-specific EEA (amol cell^{-1} h^{-1}) was calculated for LAPase, AGase, and BGase activities by dividing the respective EEA rate in the 0.2–3 µm fraction by the respective bacterial abundance.

Bacterial community composition and prediction of metabolic functions

Subsamples of 500 ml of water were filtered onto sterile polycarbonate filters in replicates (Whatman® Nuclepore™ Track-Etched Membranes diam. 47 mm, pore size 0.2 µm). Filters were placed in sterile cryogenic vials before immediate flash-freezing in liquid nitrogen and stored at −80°C. DNA extraction followed the protocol from Nercessian et al. (2005) with slight modifications (Supplemental methods S1). V3–V4 region of the 16S rRNA gene were amplified using the primer set 341F–785R (Klindworth et al. 2013) and sequenced using Illumina MiSeq 2 × 300 bp (Illumina Inc., San Diego, CA, USA). Demultiplexed and adapter clipped reads obtained from LGC Genomics were processed as mixed ones. Sequence data processing was performed according to a tailored snakemake-implemented DADA2 workflow with specific parameter settings provided as Supplementary material. 16S rRNA gene copy number correction was performed for all sequences with PICRUSt2 v.2–2.5.1 (Douglas et al. 2020). This approach aimed to use 16S sequences information to predict gene families present in the bacterial community and to combine them in order to estimate the composite metagenome in a tailored workflow (Köster et al. 2012, Callahan et al. 2016, Douglas et al. 2020), including the following steps: (i) maximum likelihood-based phylogenetic placement of sequences on a user-supplied reference tree and alignment via EPA-NG v0.3.8 (Evolutionary Placement Algorithm previously implemented in RAxML, Barbera 2019), (ii) hidden-state prediction for 16S rRNA gene copy, Enzyme Commission (EC) numbers, and Kegg Orthologs abundances per-genomes, (iii) metagenome prediction, predicted marker gene abundances and predicted gene family abundances from the amplicon sequence variants (ASVs) abundance table. The input ASVs abundance table (containing sequence abundances in read counts) was normalized by the predicted number of 16S rRNA gene copies known for each taxon. The predicted functional profiles per sample were then determined. The normalized sequence abundance table and the weighted nearest-sequenced taxon index (NSTI) values per-sample were obtained. All ASVs with NSTI > 1 were excluded from the downstream analysis. ASVs contributions were included in the output file consisting of the table with ASVs normalized by predicted 16S rRNA gene copy number abundances and predicted metabolic functions with enzymes identified by EC numbers. The ASVs occurring with a minimum relative abundance of 5% over the whole community were subsetted and then their contributions to the predicted APase (EC:3.1.3.1), α-glucosidase (EC:3.2.1.20), β-glucosidase (EC:3.2.1.21), and leucyl aminopeptidase (EC:3.4.11.1) were investigated.

Data analysis

Linear mixed effects modeling was applied to determine effects on enzymatic activities in different size fractions. Fixed explanatory variables included chlorophyll-*a*, inorganic, and organic nutrient concentrations, and the elemental ratios of organic nutrients. In addition, the effect of treatment was investigated separately for each enzyme in each size fraction. For activities of AGase, BGase, and LAPase in the bacterial size fraction (0.2–3 µm), cell-specific activities were used as response variable and cell-specific BPT was included as an additional fixed effect after Spearman's rank-order correlation was used to detect correlation between bacterial abundance and EEA in the 0.2–3 µm fraction. Mesocosm bag as factor was used as the random effect to account for dependency among measurements from the same mesocosm over time. Autocorrelation function was used to detect patterns of autocorrelation, and an appropriate autocorrelation structure was included in the model when appropriate. Model assumptions were verified by examination of residuals and the response variable was square root or $\log_{10}$-transformed prior to model refitting when required to ensure normality and homogeneity. Akaike information criteria was used in model selection and optimal models were selected based on restricted maximum-likelihood estimation criterion. Mixed effects modeling was conducted in R v.4.3.0 (R Core Team 2022) using package nlme (Pinheiro et al. 2023) and package emmeans (Length 2023) was used to obtain estimated marginal means for mixed effects models investigating the treatment effect. Uptake rate of phosphate was calculated for each treatment by linear regression (phosphate concentration versus time in days). One-way ANOVA with *post hoc* Dunnett's test was used for comparing several treatments with the control for bacterial abundance on days 6 and 8, and BPL, and BPT on experiment day 6. BPL was sqrt-transformed to ensure homogeneity and normality. Due to non-normality, the nonparametric Mann–Whitney U test was used to compare APase, AGase, BGase, and LAPase activities between the 0.2–3 µm and the >3 µm fractions during last three samplings in all treatments separately. For this, data from days 10 to 15 were pooled. Results were considered significant at $P < 0.05$. Graphs were done in the R package ggplot (Wickham 2016) and in base R with occasional postprocessing in Inkscape (Inkscape Project 2020).

Results

Temperature, chlorophyll, and inorganic nutrients

The water temperature was relatively high at the start of the experiment (~18°C). There was a temporary 5.3°C decline between days 5 and 9 caused by upwelling of cold water that cooled water inside the mesocosm bags to about 13°C. Thereafter, the temperature gradually increased to reach >20°C on the last day of the experiment (Fig. 1A). There was a steep decrease in chlorophyll-*a* concentration from ~3.4 to ~0.8 µg l^{-1} between days 0 and 3 in the control and C-treatment, and from ~3.9 to ~2.1 µg l^{-1} between days 1 and 3 in the N- and NC-treatments (Fig. 1B), which coincided with a depletion of NO_3^- (Fig. 1C). The chlorophyll-*a* concentration increased again between days 6 and 15, especially in the C-treatment. Comparison of the linear regression slopes revealed a faster uptake of PO_4^{3-} in the N- and NC-treatments (N-treatment: $r^2 = 0.93$, $P = .0027$ and NC-treatment: $r^2 = 0.89$, $P = .0015$) compared to the C-treatment and the control during the first 3 days, but P was not depleted in any treatment during the entire experiment (Fig. 1D). The remaining P at the end of the experiment was ~0.16 µmol l^{-1} and ~0.35 µmol l^{-1} in the mesocosms with N amended (N- and NC-treatment) and unamended (control and C-treatment) mesocosms, respectively. The fastest P uptake rate occurred during the first 3 days of the experiment

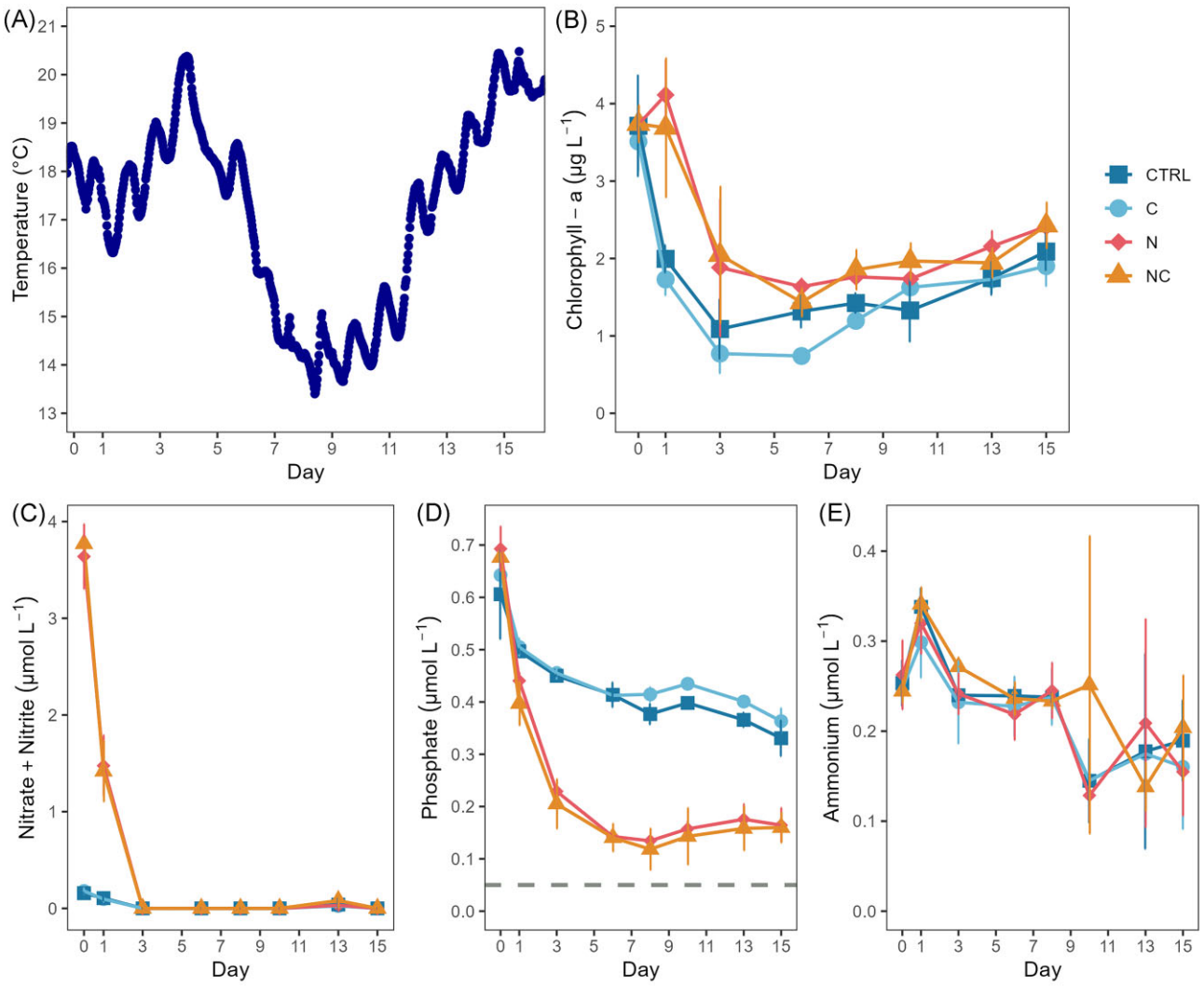

Figure 1. (A) Temperature logger data from mesocosm 1 and concentration time series of (B) chlorophyll-*a*, (C) nitrate+nitrite (µmol NO_3^-+NO_2^- l^{-1}), (D) phosphate (µmol PO_4^{3-} l^{-1}), and (E) ammonium (µmol NH_4^+ l^{-1}). Error bars represent standard deviations of triplicate mesocosm bags. Nonvisible error bars are smaller than the marker. Dashed horizontal line in (D) indicates concentration of phosphate depletion (0.05 µmol l^{-1}).

during which the added nitrate became depleted in all treatments indicating active phytoplankton growth. The ammonium concentrations declined by almost half in all mesocosms after day 1 from ~0.32 ± 0.02 µmol l^{-1} to ~0.17 ± 0.05 µmol l^{-1} on day 15 (Fig. 1E).

Dissolved and particulate organic nutrients

There was no significant treatment effect on concentrations of DOC (P > .259; Supplementary Table S1), DON (P > .117; Supplementary Table S1), and DOP (P > .659, Supplementary Table S1) (Fig. 2A–C). DOC concentrations were relatively stable throughout the experiment (~0.52 ± SD 0.05 mmol l^{-1}), whereas DON concentrations showed a pattern of production and removal. DON increased in all treatments during the first 3 days of the experiment (Fig. 2B), when the uptake of nitrate+nitrite was fast (Fig. 1C). At the end of the experiment, on average, DON concentration was 3.6 µmol l^{-1} higher compared to the start of the experiment, indicating accumulation of refractory DON. The DOP concentration increased from ~0.36 ± 0.03 µmol l^{-1} to ~0.45 ± 0.04 µmol l^{-1} between days 1 and 6, after which the DOP decreased close to the starting concentration ~0.35 ± 0.03 µmol l^{-1} at the end of the experiment (Fig. 2C).

The DOC:DON ratio ranged between 17 and 31 without any clear differences among treatments (Fig. 2D). Both DOC:DOP and DON:DOP ratios decreased until the mid-experiment, and thereafter increased similarly in all treatments towards the end of the experiment (Fig. 2E and F).

The PON concentration was significantly higher in the N-treatment compared to the control (P = .0395; Supplementary Table S1) and C-treatment (P = .0269; Supplementary Table S1) and NC-treatment had significantly higher PON concentration compared to C-treatment (P = .0442; Supplementary Table S1). POP concentration was significantly higher in the N- and NC-treatments compared to the control (P_N = .0044 and P_{NC} = .0057; Supplementary Table S1) and C-treatment (P_N = .0009 and P_{NC} = .0012; Supplementary Table S1). In the control and C-treatment the steepest decrease of all particulates occurred during the first half of the experiment after which the concentrations stabilized during the latter phase of the experiment (Fig. 2G–I). For both POC and POP in the N- and NC-treatments, the decrease was slower compared to the C-treatment and the control but

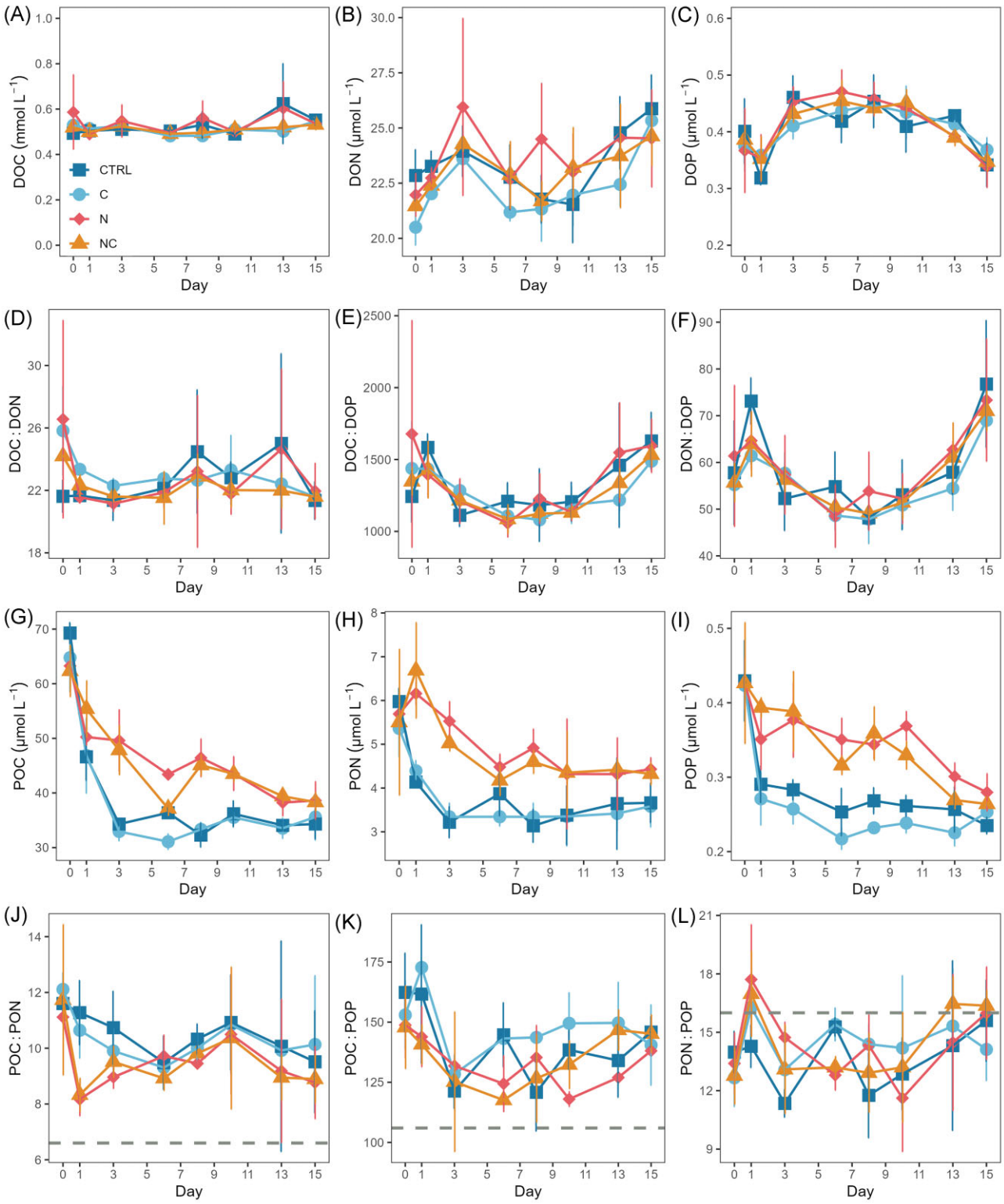

Figure 2. Concentrations of (A) DOC, (B) DON, (C) DOP, and (D–F) stoichiometric ratios of dissolved organic nutrients over time. (G) POC, (H) PON, (I) POP, and (J–L) stoichiometric ratios of particulate organic nutrients over time. Horizontal gray dashed lines in panels (J–L) indicate molar Redfield ratios. Error bars represent standard deviations of triplicate mesocosm bags. Nonvisible error bars are smaller than the marker.

constant throughout the entire experiment. The PON concentration decreased during the first 3 days of the experiment as the DON concentration increased, and the uptake of nitrate+nitrite was fast.

The POC:PON and the POC:POP ratios were higher than the Redfield values 6.6 and 106, respectively, while the PON:POP ratios were below the Redfield value (16) almost throughout the entire experiment (Fig. 2J–L).

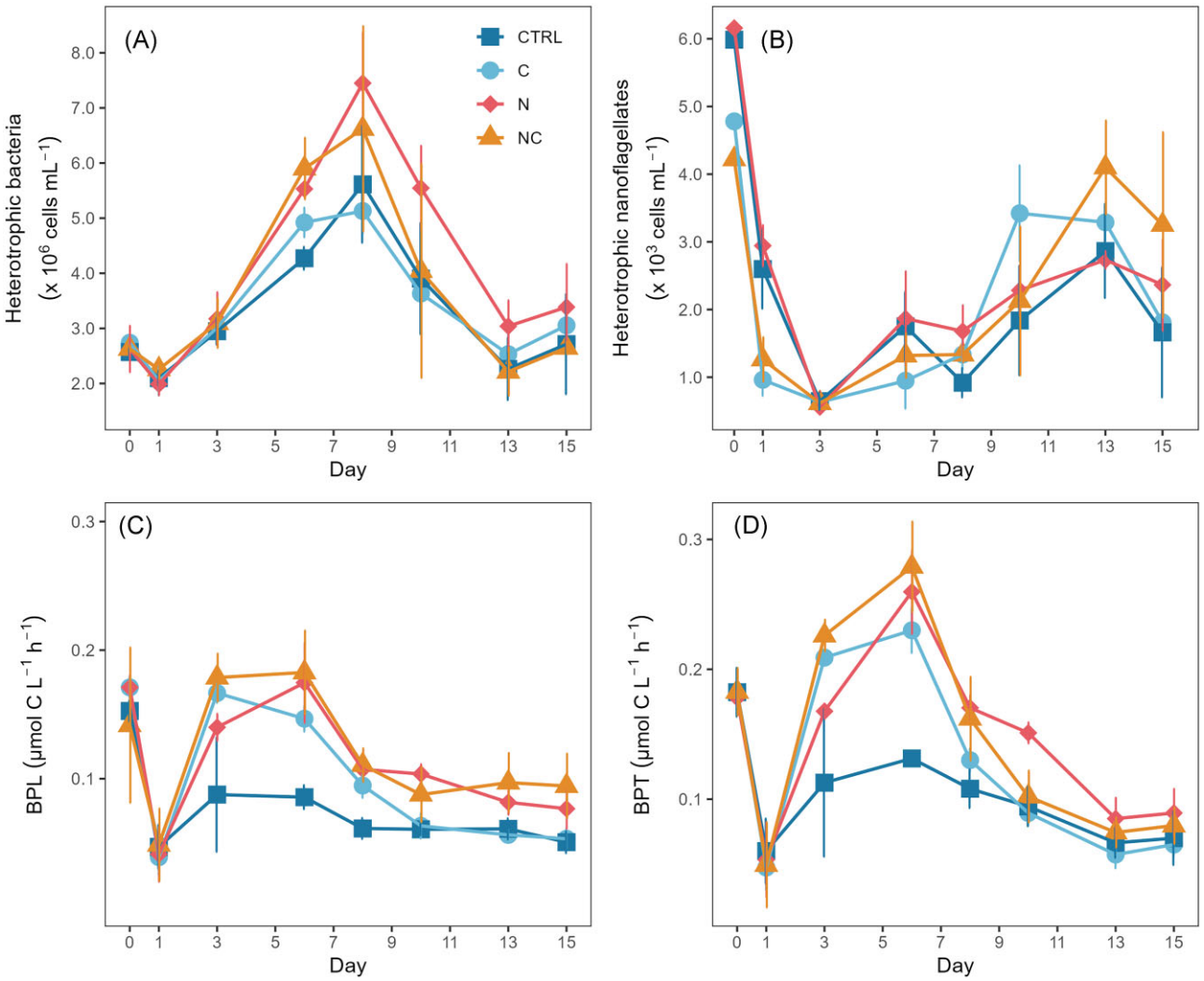

Figure 3. (A) Abundance of heterotrophic bacteria, (B) heterotrophic nanoflagellates and bacterial production measured as (C) leucine incorporation (BPL) and (D) thymidine incorporation (BPT) over time. Error bars represent standard deviations of triplicate mesocosm bags. Nonvisible error bars are smaller than the marker.

Biovolume

The contribution of detritus to the total biovolume generally decreased in all treatments during the first half of the experiment from ~54.1% to ~27.7% after which it increased again toward the end of the experiment (Supplementary Fig. S1). Lowest mean contribution of detritus to the total biovolume was observed in the NC-treatment on day 8 (18.6%). The results of the FlowCam measurements are presented in Spilling et al. (2024).

Bacterial abundance and production

Different treatments started to show varying effects on heterotrophic bacteria after day 3 and the abundance peak occurred on day 8 in all treatments, which was 2–5 days after the bacterial production maximum (Fig. 3). The highest average abundances of heterotrophic bacteria occurred in treatments with N- and NC-additions on day 8, 7.4 × 10^6 cells ml^{-1} and 6.6 × 10^6 cells ml^{-1}, respectively, but the difference among treatments was not significant (One-way ANOVA: P = .153; Supplementary Table S2). On day 6, bacterial abundance was significantly higher in N- and NC-treatment compared to the control (Dunnett's test: $P_{\text{N-treatment}}$ = .0044, $P_{\text{NC-treatment}}$ = .0006; Supplementary Table S2), but there was no significant difference between the control and C-treatment (Dunnett's test: $P_{\text{C-treatment}}$ = .1029; Supplementary Table S2). A sharp drop in bacterial abundance occurred soon after the peak and the bacterial abundance was generally similar during the first and last samplings. Bacterial production increased in all treatments after an initial drop between the start and day 1 but was lower in the control compared to all other treatments (Fig. 3C and D). During the bacterial production peak on day 6, BPT was significantly higher in all other treatments compared to the control (Dunnett's test: $P_{\text{C-treatment}}$ = .0035, $P_{\text{N-treatment}}$ = .0004, and $P_{\text{NC-treatment}}$ = .0004; Supplementary Table S2) and the same was observed for BPL (Dunnett's test: $P_{\text{C-treatment}}$ = .0117, $P_{\text{N-treatment}}$ = .0020, and $P_{\text{NC-treatment}}$ = .0012; Supplementary Table S2). After day 6, bacterial production decreased to lower levels than at the start of the experiment. BPL stagnated at slightly higher level in N and NC-treatments whereas the treatment effect in BPT had faded by day 13.

Heterotrophic nanoflagellates

There was an order of magnitude decline in abundance of heterotrophic nanoflagellates from ~5000 cells ml^{-1} to ~600 cells ml^{-1} between experiment days 0 and 3 (Fig. 3B). After day 3, the

abundance started to increase toward the end of the experiment concomitantly with the decline of the abundance of heterotrophic bacteria after the peak on day 8.

Development and drivers of extracellular enzyme activities

Similar to bacterial production (Fig. 3C and D), the temporal development of bacterial abundance followed closely the activities of AGase (Spearman's rank correlation, $r = 0.67$, $P < .0001$; Supplementary Table S2), BGase (Spearman's rank correlation, $r = 0.64$, $P < .0001$; Supplementary Table S2), and LAPase (Spearman's rank correlation, $r = 0.77$, $P < .0001$; Supplementary Table S2) in the fraction 0.2–3 µm with a lag of two days (Fig. 4). LAPase had the highest hydrolytic rates compared to other enzymes. During the first half of the experiment, activities of AGase, BGase, and LAPase were predominant in the bacterial (0.2–3 µm) fraction (Fig. 4) and the cell-specific AGase, BGase, and LAPase showed two distinctive peaks during the experiment: the first one on days 3–5 and the second one after day 10 (Fig. 5). Cell-specific BPT correlated positively with cell-specific AGase, BGase, and LAPase activities (for all $P < .0001$; Supplementary Table S3). In addition, both cell-specific glycolytic enzyme activities were negatively affected by the DOC:DON ratio ($P_{AGase} = .0008$ and $P_{BGase} = .0003$; Supplementary Table S3). Cell-specific LAPase activity was negatively affected by DOC concentration ($P = .0077$; Supplementary Table S3) and positively affected by DON concentration ($P = .0112$; Supplementary Table S3). There was no temporal congruence between APase activity in the 0.2–3 µm fraction and bacterial abundance (Spearman's rank correlation, $r = 0.03$, $P = .77$; Supplementary Table S2). DIP ($P < .0001$; Supplementary Table S3) and POP ($P < .0001$; Supplementary Table S3) had a positive effect on APase activity in 0.2–3 µm fraction whereas there was a significant negative effect of chlorophyll-*a* ($P = .0004$; Supplementary Table S3) on APase activity.

The dissolved APase fraction accounted for the largest share of total APase activity throughout the experiment (on average 60.3%) (Supplementary Fig. S2). With a slight increase after the mid experiment, the dissolved fraction was the only fraction of APase activity that did not show a decreasing trend over time (Fig. 4). The dissolved APase activity was positively affected by chlorophyll-*a* concentration ($P = .0001$; Supplementary Table S3) and negatively by DOP concentration ($P = .0218$; Supplementary Table S3). In contrast to high dissolved APase activity, activities of dissolved glucosidases were negligible (Fig. 4 and Supplementary Fig. S2) and the dissolved LAPase activity was substantially lower compared to other fractions constituting 4%–15% of total LAPase activity. In addition, it showed a slight decreasing trend over time without any treatment effect (Fig. 4). Dissolved LAPase displayed a significant positive relationship with NH_4^+ concentration ($P = .0014$; Supplementary Table S3) and a negative response to DON:DOP ratio ($P = .0197$; Supplementary Table S3).

Peptidolytic rates in the >3 µm fraction increased over time with slightly higher LAPase rate in the NC-treatment (Fig. 4F), but the treatment effect was insignificant. When only the last three samplings were considered, LAPase activity was significantly higher in the >3 µm fraction compared to the 0.2–3 µm fraction in the NC-treatment (Mann–Whitney: $P = .001$; Supplementary Table S2). LAPase activity in the >3 µm fraction showed a significant negative response to NH_4^+ concentration ($P = .0017$; Supplementary Table S3) and POC:PON ratio ($P = .0016$; Supplementary Table S3). Glycolytic activities in the >3 µm fraction had a clear peak in the NC-treatment on experiment day 3 and a shorter peak on day 13 (Fig. 4). For the AGase activities in fraction >3 µm, the NC-treatment displayed significantly higher rates compared to the control ($P = .0259$; Supplementary Table S4), the N-treatment ($P = .0216$; Supplementary Table S4), and the C-treatment ($P = .0067$; Supplementary Table S4), while BGase activity in the NC-treatment was significantly higher only in comparison to the control ($P = .0177$; Supplementary Table S4). In addition, when the last three samplings were considered, AGase activity was higher in the >3 µm fraction compared to the 0.2–3 µm fraction in the NC-treatment (Mann–Whitney: $P = .017$; Supplementary Table S2), but this was not the case for BGase. None of the explanatory variables significantly affected AGase or BGase in the >3 µm fraction. Significantly higher APase activities were detected in the >3 µm fraction compared to the 0.2–3 µm fraction in the NC-treatment (Mann–Whitney: $P = .006$; Supplementary Table S2) during the last three samplings. The significant variables affecting APase activity in the >3 µm fraction were POP concentration and POC:POP ratio with a positive correlation ($P_{POP} < .0001$, $P_{POC:\ POP} = .0133$; Supplementary Table S3).

Bacterial community structure and functional predictions

Based on 16S rRNA gene sequences, the dominant classes over the experiment were Acidimicrobiia, Actinobacteria, Alphaproteobacteria, Bacteroidia, Bacilli, Cyanobacteria, Gammaproteobacteria, Planctomycetes, and Verrucomicrobiae (Fig. 6). During the first half of the experiment, Actinobacteria was the dominating bacterial class with an abundance ranging between 39% on day 0 and 36% on day 3 across all mesocosms followed by a decrease in relative abundance of Alphaproteobacteria from 21% on day 3 to 17% on day 6 and a slight increase in relative abundance of Bacteroidia from 17% on day 3 to 21% on day 6. In the second half of the experiment, an increase in relative abundance was observed for the classes Cyanobacteria ranging between 10% on day 8 and 22% on day 15, Gammaproteobacteria between 16% on day 8, and 18% on day 15, and Planctomycetes from 3% on day 10 to 5% on day 15. Simultaneously, a decrease in abundance of Actinobacteria from 31% to 10% between days 8 and 15 was observed. ASVs contributions to the predicted metabolic activities of LAPase, AGase, BGase, and APase were investigated with the aim to describe the interplay between the most abundant bacterial taxa and the predicted metabolic processes within the community (Table 1). The correction by 16S rRNA gene copy number and the phylogenetic placement into a reference tree of the identified ASVs allowed a taxonomy-informed prediction of each enzymatic activity via PICRUST 2 (Douglas et al. 2020). This resulted in fifteen ASVs predicted to encode LAPase, AGase, and BGase whereas six ASVs were predicted to encode APase. Nearly the same ASVs contributed to the predicted LAPase, AGase, and BGase activities, except for ASV1 classified as *Cyanobium gracile* PCC 6307 and ASV3 and ASV6 classified as *Candidatus* Limnoluna that only contributed to the predicted LAPase and AGase activities. The ASVs contributing to the predicted activities changed consistently with the succession of the bacterial community with a clear transition of the functional composition on day 8 of the experiment (Table 1). In general, ASVs classified as *Sporichthyaceae* (Actinobacteria) and *Pseudorhodobacter* (Alphaproteobacteria) contributed to the predicted LAPase, AGase, and BGase activities during the first half of the experiment (days 1–6) when the measured activities of these enzymes increased and peaked (Fig. 4). In addition, *Candidatus* Limnoluna (ASV3 and ASV6, Actinobacteria) contributed most to the predicted AGase activity on days 1–6. Contribution of *C. gracile* PCC 6307

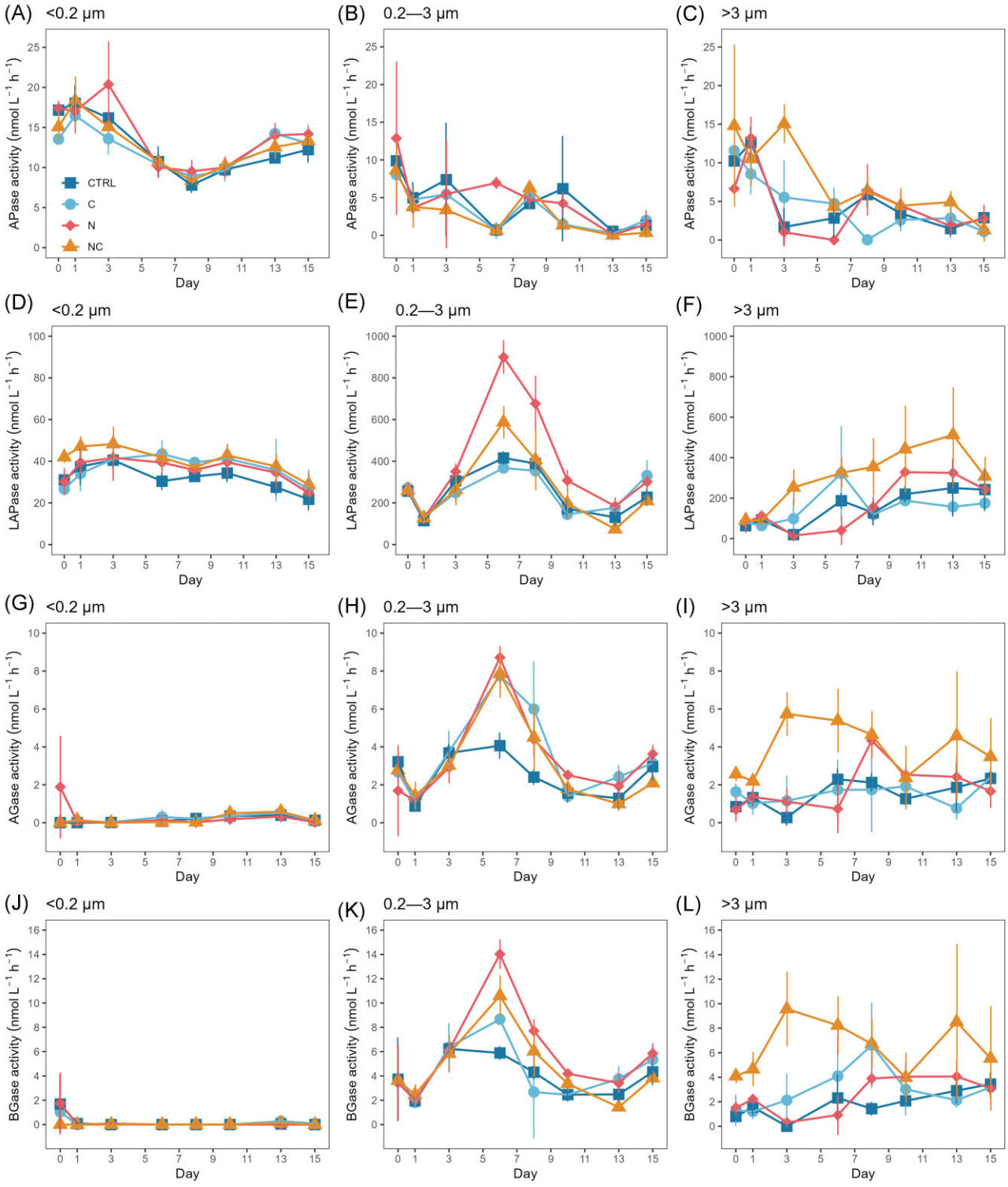

Figure 4. Potential hydrolytic activities (nmol l^{-1} h^{-1}) of (A–C) APase, (D–F) leucine aminopeptidase (LAPase), (G–I) α-glucosidase (AGase), and (J–L) β-glucosidase (BGase) in three fractions (A, D, G, and J) < 0.2 µm, (B, E, H, and K) 0.2–3 µm, and (C, F, I, and L) > 3 µm. Note that the scale for LAPase (D) is an order of magnitude lower than for the two other fractions (E and F). Error bars represent standard deviations of triplicate mesocosm bags. Nonvisible error bars are smaller than the marker.

(Cyanobacteria) to the total predicted LAPase and BGase activities increased on days 8, 13 and 15 (up to 16% of the community-wide function abundance). The groups contributing to the community-wide predicted activities at the end of the experiment differed from the ones present at the beginning, although they also included representatives from classes Actinobacteria and Alphaproteobacteria (Table 1). Furthermore, their contribution to the community-wide predicted activity was generally lower than the ones predicted for other taxa at the start of the experiment. *Pseudohongiella* (Gammaproteobacteria) and *Isosphaeraceae*

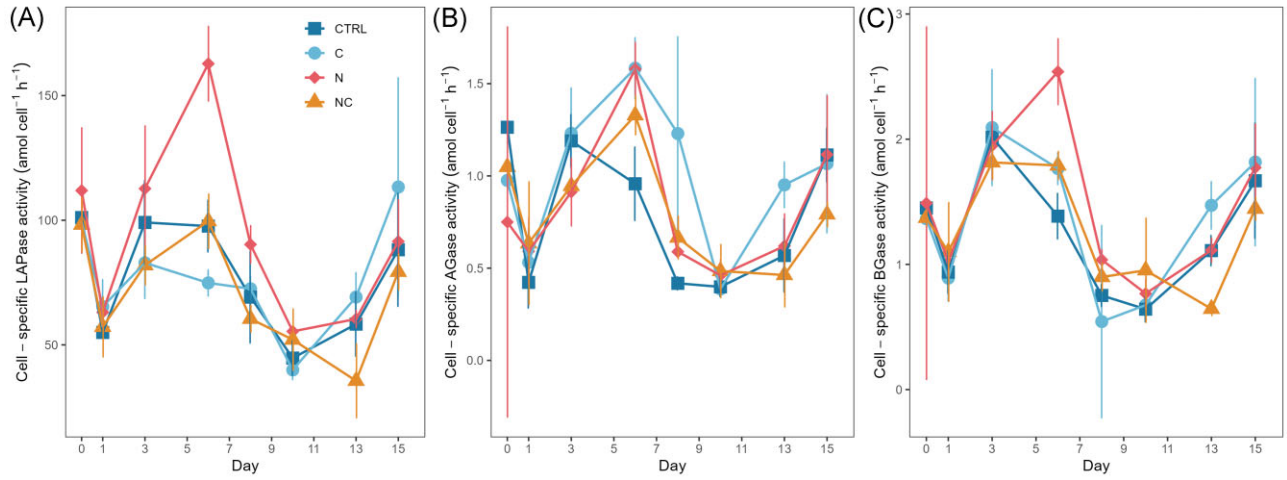

Figure 5. The development of cell-specific extracellular enzyme activities of (A) leucine-aminopeptidase (LAPase), (B) α-glucosidase (AGase), and (C) β-glucosidase (BGase) in the size fraction 0.2–3 µm. Error bars represent standard deviations of triplicate mesocosm bags. Nonvisible error bars are smaller than the marker.

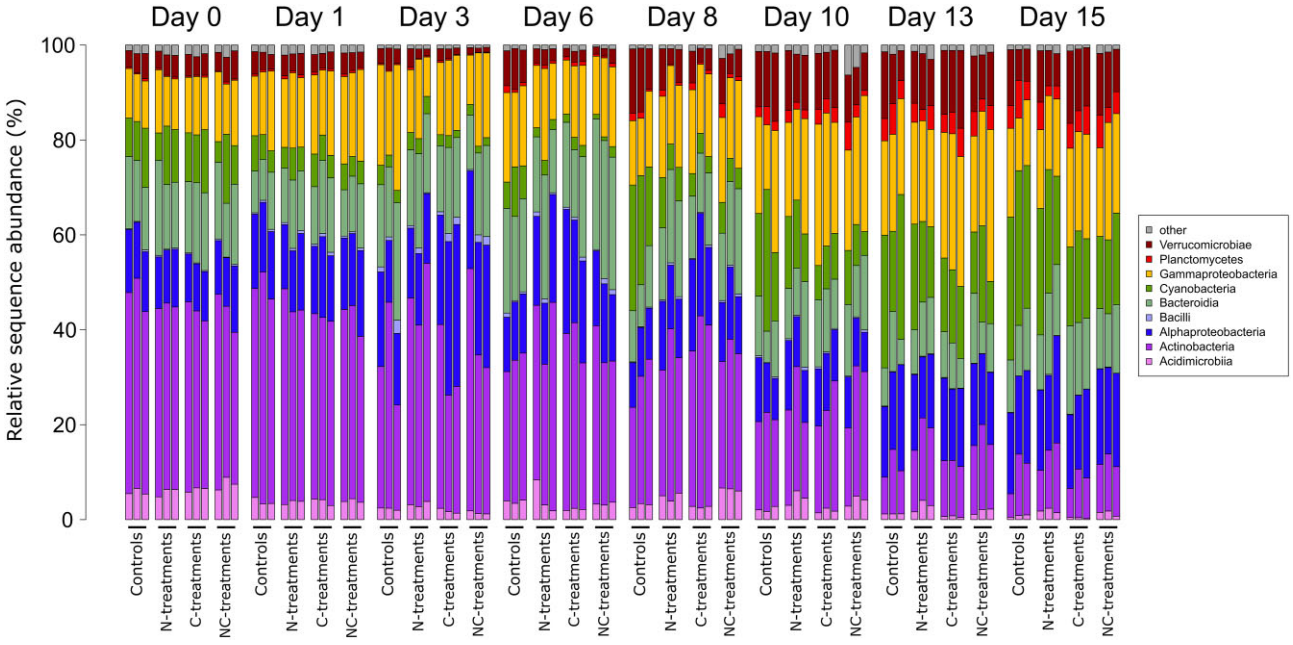

Figure 6. Temporal development of the 10 most abundant classes of the bacterial community.

(Planctomycetes) contributed to the predicted activities only during the last sampling days.

Discussion

The aim of this study was to investigate the possible drivers of EEAs and the degradation potential of OM, which is crucial in determining the utilization of the excess phosphate pool following the northern Baltic spring bloom. In addition, measured EEAs were compared with predicted functions identified with their corresponding enzymatic activities based on 16S rRNA gene sequences of the bacterial community.

Fate of excess phosphate

Although the excess phosphate pool decreased in all treatments, it was not depleted during our experiment contradicting findings of a previous longer study in the Tvärminne archipelago (Vanharanta and Spilling 2023). APase activity has typically been used as an indicator of physiological P limitation of microbes (Nausch and Nausch 2004, Mahaffey et al. 2014, Baltar et al. 2016), but it can also be used for carbon acquisition in phosphate replete systems (Hoppe 2003). The hydrolytic rates of bulk APase measured in our study under phosphate replete conditions (12.3–44.4 nmol l^{-1} h^{-1}) were comparable to the activities measured in May–June in the western Baltic Proper (0–31.9 nmol l^{-1} h^{-1}) that were associated with P limitation (Baltar et al. 2016). It is plausible that the hydrolytic rates measured in our study had been relicts from P-limiting conditions before the start of the experiment as indicated by DIP concentration below the threshold of 0.03 µmol l^{-1} known to induce APase production (Mahaffey et al. 2014) and the decreasing trend of APase in the two larger fractions over time. This finding demonstrates the long extracellular lifetime of

Table 1. List of ASVs that contributed to the predicted enzymatic activities (expressed as relative abundance of metabolic functions) throughout the experiment with ranges between minimum and maximum values. Column *n* indicates the number of mesocosms, where the respective taxon occurred. Column Taxonomy indicates the lowest classified taxonomic level for each ASV. The symbol "–" indicates a lower contribution than 5% of an ASV to the predicted enzymatic activity.

ASV	Treatment	*n*	Class	Taxonomy	Predicted LAPase %	Predicted AGase %	Predicted BGase %	Predicted APase %
Day 0								
ASV1	Ctrl, C, N, NC	7	Cyanobacteria	*Cyanobium gracile* PCC 6307	6.1–9.1	–	6.1–9.1	–
ASV2	Ctrl, NC	2	Alphaproteobacteria	*Pseudorhodobacter*	10.8–13.1	5.4–6.5	5.4–6.5	–
ASV3	Ctrl, N, NC	4	Actinobacteria	*Candidatus* Limnoluna	5.2–5.9	15.6–17.8	–	–
ASV4	Ctrl, C, N, NC	11	Actinobacteria	*Sporichthyaceae*	10.1–14.7	10.1–14.7	5.0–7.3	–
Day 1								
ASV2	C, NC	5	Alphaproteobacteria	*Pseudorhodobacter*	10.2–14.6	5.1–7.3	5.1–7.3	–
ASV3	Ctrl, C, N, NC	12	Actinobacteria	*Candidatus* Limnoluna	5.7–8.7	17.0–26.2	–	–
ASV4	Ctrl, C, N, NC	12	Actinobacteria	*Sporichthyaceae*	10.2–14.1	10.2–14.1	5.1–7.0	–
ASV6	Ctrl, N	3	Actinobacteria	*Candidatus* Limnoluna	5.0–5.7	15.2–17.1	–	–
Day 3								
ASV2	Ctrl, C, N, NC	8	Alphaproteobacteria	*Pseudorhodobacter*	11.0–33.3	5.5–16.6	5.5–16.6	–
ASV3	Ctrl, C, N, NC	10	Actinobacteria	*Candidatus* Limnoluna	5.4–11.7	16.2–35.2	–	–
ASV4	Ctrl, C, N, NC	8	Actinobacteria	*Sporichthyaceae*	10.2–16.6	10.2–16.6	5.1–8.3	–
ASV6	Ctrl, C, N, NC	4	Actinobacteria	*Candidatus* Limnoluna	5.4–6.6	16.1–20.0	–	–
ASV18	Ctrl, C, N, NC	8	Bacteroidia	*Cryomorphaceae*	5.2–10.0	5.2–10.0	5.2–10.0	5.2–10.0
Day 6								
ASV1	Ctrl	1	Cyanobacteria	*Cyanobium gracile* PCC- 6307	5.2	–	5.2	–
ASV2	C, N, NC	8	Alphaproteobacteria	*Pseudorhodobacter*	11.9–30.2	6.0–15.1	6.0–15.1	–
ASV3	Ctrl, C, N, NC	6	Actinobacteria	*Candidatus* Limnoluna	5.2–6.1	15.5–18.4	–	–
ASV4	N	1	Actinobacteria	*Sporichthyaceae*	11.5	5.7	5	–
ASV5	N	1	Bacteroidia	*Fluviicola*	5.2	–	5.2	5.2
ASV6	N, NC	3	Actinobacteria	*Candidatus* Limnoluna	5.3–5.6	16.0–16.7	–	–
Day 8								
ASV1	Ctrl, N	4	Cyanobacteria	*Cyanobium gracile* PCC- 6307	5.6–16.4	–	5.6–16.4	–
ASV2	C	2	Alphaproteobacteria	*Pseudorhodobacter*	15.0–17.4	7.5–8.7	7.5–8.7	–
ASV3	N	1	Actinobacteria	*Candidatus* Limnoluna	6.0	18.1	–	–
ASV4	N	1	Actinobacteria	*Sporichthyaceae*	10.3	10.3	5.1	–
ASV5	N	1	Bacteroidia	*Fluviicola*	7.2	–	7.2	7.2
ASV37	Ctrl	1	Verrucomicrobiae	*Roseibacillus*	–	–	6.1	12.2
Day 10								
ASV1	Ctrl, N	6	Cyanobacteria	*Cyanobium gracile* PCC- 6307	5.3–11.7	–	5.3–11.7	–
ASV9	Ctrl	1	Cyanobacteria	*Cyanobium gracile* PCC- 6307	5.3	–	10.7	–
Day 13								
ASV1	Ctrl, C, N, NC	10	Cyanobacteria	*Cyanobium gracile* PCC- 6307	5.0–15.0	–	5.0–15.0	–
ASV7	C, NC	3	Gammaproteobacteria	*Pseudohongiella*	5.1–6.0	–	–	10.1–12.0
ASV11	Ctrl, C	2	Alphaproteobacteria	SAR 11 (clade III)	5.5–9.5	–	–	–
ASV12	NC	1	Cyanobacteria	*Cyanobium gracile* PCC- 6307	5.1	–	5.1	–
Day 15								
ASV1	Ctrl, C, N, NC	9	Cyanobacteria	*Cyanobium gracile* PCC- 6307	5.3–16.0	–	5.3–16.0	–
ASV7	C	1	Gammaproteobacteria	*Pseudohongiella*	5.6	–	–	11.2
ASV8	Ctrl	1	Planctomycetes	*Isosphaeraceae*	6.9	–	–	13.8
ASV10	N, NC	3	Alphaproteobacteria	*Rhodobacteraceae*	10.5–11.7	5.3–5.8	5.3–5.8	–
ASV22	N, NC	2	Actinobacteria	*Mycobacterium*	5.0	5.0	5.0	–
ASV52	Ctrl, C, N, NC	4	Bacteroidia	*Cryomorphaceae*	5.4–8.6	5.4–8.5	5.4–8.6	5.4–8.6

these enzymes (Thomson et al. 2019). In other P-limited aquatic environments, however, many-fold higher APase activities have been reported, e.g. Lake Constance (115 nmol l^{-1} h^{-1}; Grossart and Simon 1998), the southern Baltic Sea (543 nmol l^{-1} h^{-1}; Nausch et al. 1998), Florida Bay (1220 nmol l^{-1} h^{-1}; Koch et al. 2009), and the Adriatic Sea (2916 nmol l^{-1} h^{-1}; Ivančić et al. 2016) demonstrating the difficulty in relating EEAs to nutrient deficiency of bacterial communities and to compare enzymatic hydrolytic rates across different aquatic ecosystems.

We detected an increase of ∼0.2 µmol of DOP l^{-1} during the first half of the experiment, which was mineralized between days 6 and 15 although phosphate was still available. It is probable that dissolved APase, constituting the majority of the total APase activity (44%–90%; Supplementary Fig. S2), contributed to the observed decrease in DOP concentration after mid experiment, and thereby to excess phosphate concentrations. The possible source for dissolved APase during the second half of the experiment are carbon-limited heterotrophic bacteria known to secrete APase into the solution (Luo et al. 2009). This is corroborated by the metabolic prediction results that showed an increasing contribution to the predicted APase activity of bacterial ASVs after day 8 (Table 1). In particular, ASVs in classes Verrucomicrobiae and Planctomycetes seemed to require more phosphorus compared to other ASVs (Table 1). Sloppy feeding by heterotrophic nanoflagellates or lytic viral infection could also liberate enzymes to the water and at the same time recycle nutrients bound in bacterial biomass. We did not measure viral abundances, but the development of the main grazers of picoplankton, heterotrophic nanoflagellates, increased toward the end of the study and probably also contributed to the excess phosphate pool.

The highly significant correlation between chlorophyll-*a* and dissolved APase does probably not imply causation as phytoplankton are not expected to produce APase under phosphate replete conditions. Given the absence of correlation between APase activity in the size range 0.2–3 µm and bacterial abundance and the negative correlation with chlorophyll-*a* (Supplementary Table S3), it seems reasonable that most APase activity in this size fraction was not related to free-living bacteria or small phytoplankton, but probably attributed to dissolved enzymes absorbed to small abiotic surfaces, although the true origin of APase cannot be confirmed. Furthermore, the positive correlation between APase activity in the fraction >3 µm and POP concentration and the POC:POP ratio (Supplementary Table S3) could indicate enzymatic APase activity from particle attached bacteria.

Nitrogen and carbon deficient free-living heterotrophic bacteria

The role of heterotrophic bacteria in excess phosphate utilization was of specific interest due to their generally higher affinity for phosphate uptake compared to algae (e.g. Vadstein et al. 2003) and low C:P ratio (Chrzanowski and Kyle 1996, Heldal et al. 1996). Their abundance peak around day 8 occurred after the peaks of bacteria-specific glycolytic and peptidolytic activities and bacterial production, which reached relatively high rates compared to recent studies in the Baltic Sea (Bunse et al. 2019, Camarena-Gómez et al. 2020, Zhao et al. 2023). It was technically not possible to measure bacterial activities at *in situ* temperature during the experiment but a fixed temperature of 17°C was used instead. Therefore, EEAs and bacterial production rates might be slightly overestimated during the upwelling event, which decreased temperature inside the mesocosm bags in the middle of the experiment. This could imply that without such temperature decrease slowing down bacterial activities *in situ*, more phosphate might have been taken up during the experiment. This hypothesis is supported by previous research demonstrating the effect of temperature on phosphate drawdown (Vanharanta and Spilling 2023).

AGase, BGase, and LAPase activities in the 0.2–3 µm fraction showed a similar temporal pattern and were clearly related to the bacterioplankton development whereas APase was not (Figs 3A, 4B, E, H, and K). There are likely some particle-attached bacteria also in the 0.2–3 µm fraction that were not quantified in this experiment. Consequently, there might be a slight overestimation of the cell-specific activities as the activity of 0.2–3 µm fraction was normalized to counts of free-living bacteria. However, the strong correlation between glycolytic and peptidolytic activities in the size fraction 0.2–3 µm and the bacterial abundance suggests that those activities mainly derived from free-living bacteria. The most abundant bacterial taxa were responsible for the contribution of both peptidolytic and glycolytic predicted activities (Table 1), which further demonstrates that degradation of N and C were tightly coupled also at the organismic level.

Cell-specific BPT showed a significant response with cell-specific LAPase, BGase, and AGase activities demonstrating a tight coupling between substrate degradation and uptake. These findings suggest that growth of heterotrophic bacteria, especially of taxa belonging to the class Actinobacteria, was driven by hydrolysis of N- and C-rich OM indicating inorganic nitrogen and labile carbon deficiency, which was compensated by utilizing available high molecular weight substrates that are typically associated with senescent phytoplankton and termination of phytoplankton blooms (Chróst 1991, Middelboe et al. 1995). Members of Actinobacteria are known to contribute to N and C cycling by degrading chitin that can derive from phyto- and zooplankton (Tada and Grossart 2014). Negative response of cell-specific glycolytic activities to DOC:DON ratio further supports this interpretation (Supplementary Table S3). Consistently with our results, Actinobacteria are known to occur in postbloom conditions especially in the less saline northern Baltic Sea (Hugerth et al. 2015, Rieck et al. 2015, Bunse et al. 2016) and to incorporate thymidine (Piwosz et al. 2013).

Bacterial LAPase rates in our study were several times higher compared to those measured in most previous studies, but in line with bulk LAPase activities in the Peruvian coastal upwelling system (200–800 nmol l^{-1} h^{-1}; Spilling et al. 2023), which is an oxygen minimum zone with a low DIN:DIP ratio. In the northern Baltic, postspring-bloom low DIN:DIP conditions, high N_2-fixation and degradation of N-rich organic compounds can potentially support the drawdown of excess phosphate. During our experiment, regenerated production likely prevailed due to the low abundance of large N_2-fixing filamentous cyanobacteria (filament counts available in Vanharanta et al. 2024). Based on previous research by Nausch (2000), we assume that under excess phosphate and organic nitrogen substrate availability, heterotrophic bacteria might utilize OM as inorganic nitrogen and energy source by enhancing the hydrolytic rates of peptidolytic and glycolytic enzymes. The added DIN seemed to be transformed quickly into DON, which was then utilized presumably by the free-living bacteria showing increasing LAPase rates during the first half of the experiment (Fig. 4E). Bacterial grazing of heterotrophic nanoflagellates may explain the increasing DON concentration during the second half of the experiment (Fawcett and Ward 2011).

Labile DOC has a turnover of ∼3 days (Hansell et al. 2013). Although sole glucose addition enhanced BPT and BPL (Supplementary Table S2), bacterial abundance was not significantly higher in the C-treatment compared to the control

during the bacterial abundance peak on experiment day 8 (Fig. 3A, Supplementary Table S2). This notion, together with relatively high glycolytic activities in the C-amendment, indicate that the added glucose was rapidly utilized for protein synthesis and reproduction. The addition of nitrogen in N- and NC-treatments resulted in slightly delayed or prolonged peaks in BPL and BPT likely attributed to algal-derived DOC. High LAPase activity might have alleviated the carbon demand of heterotrophic bacteria as the degradation of peptides by LAPase is not only utilized for acquiring N but also for providing C (Ylla et al. 2012). During postspring-bloom conditions, the bacterial community could be well-adapted to utilizing algal-derived polymeric substrates (Eigemann et al. 2022, Villena-Alemany et al. 2024). ASVs belonging to the class Bacteroidia that are typically linked to the degradation of high molecular weight OM in the ocean (Kirchman 2002, Lapébie et al. 2019), contributed to the predicted glycolytic activities in our experiment. However, their contribution to the total predicted BGase and AGase activities ranged only between 5.2% and 10.0%, although their relative abundance was quite high (~21%) on day 6. In addition, *Rhodobacteraceae*, a group in the order Rhodobacterales known to utilize recalcitrant OM (Allers et al. 2007), appeared at the end of the experiment.

These changes in bacterial community composition alone are insufficient to imply bottom-up control of heterotrophic bacteria. In addition, grazing by heterotrophic nanoflagellates was undoubtedly an important factor influencing bacterial numbers during the latter half of the experiment (Fig. 3). However, the relative 16S rRNA sequence abundance of Cyanobacteria increased toward the end of the experiment (Fig. 6). This trend was also to some extent mirrored in picocyanobacterial cell numbers, which increased after nitrate was depleted (Spilling et al. 2024). A comparable increase was observed also for picoeukaryotes (Spilling et al. 2024). Heterotrophic bacteria and picoautotrophs compete for inorganic nutrients, yet the crucial functional difference governing uptake of nutrients lies in the source of energy i.e. labile organic carbon and light, respectively. Our findings may therefore indicate that in addition to grazing loss, heterotrophic bacteria were also constrained by the availability of labile energy sources. This probable limitation potentially provided competitive advantage for autotrophic picoplankton.

Substrate availability-induced changes in microbial enzymatic activities

In the NC-treatment, significantly higher rates of AGase, and BGase activities in the >3 µm fraction likely resulted from a higher biovolume (including detritus) (Supplementary Fig. S1A) serving as a surface for microbial colonization and enhanced EEAs (Simon et al. 2002). The ability of particle-attached bacteria to exploit a wider variety of polymeric C-substrates compared to their free-living counterparts (Lyons and Dobbs 2012) has been shown to result in higher enzymatic activities on aggregates than in the surrounding water (e.g. Grossart et al. 2003). However, our results contradict with several studies that showed higher EEAs of particle-attached bacteria compared to free-living ones (Karner and Herndl 1992, Smith et al 1992, Grossart et al. 2007b), as activities of LAPase, AGase, and BGase in the size fraction >3 µm were comparable or generally lower than those measured in the 0.2–3 µm fraction (Fig. 4) during the first half of the experiment.

Although the abundance of particle-attached bacteria was not counted, it is possible that, per sample volume, numbers of free-living bacteria exceeded those attached to aggregates at the beginning of the experiment. This could be attributed to high sedimentation losses observed as decreasing POM concentrations during the first days of the experiment. Such decrease was likely the consequence of sedimentation of microphytoplankton, particularly diatoms, as indicated by declining BSi concentration (Spilling et al. 2024) and presumable senescence of large (>10 µm) dinoflagellates after nitrate depletion (Heiskanen 1998, Tamelander and Heiskanen 2004, Spilling et al. 2018). The disintegration of phytoplankton probably provided degradable DOM that might have favored the growth of the free-living bacteria. Bacterial growth on aggregates can also be balanced by intensive grazing of protozoans (Ploug and Grossart 2000) or even mesozooplankton (e.g. Steinberg et al. 2008). The detected increase in the abundance of copepods toward the end of the experiment (Spilling et al. 2024) and observations of suspected large, fragmented copepod fecal pellets (Supplementary Fig. S3) would, however, rather imply recycling of fecal organic material and retention of nutrients in the surface.

It is also likely that particle-attached and free-living bacterial fractions differ phylogenetically and functionally from each other (Lyons and Dobbs 2012, Mohit et al. 2014, Rieck et al. 2015), which could lead to distinct enzymatic activities between both fractions (Azúa et al. 2003). Temporal succession of ASVs contributing to the predicted activities seemed to reflect a change from bacteria in the free-living to the particle-attached fraction. For instance, several ASVs classified as *Pseudorhodobacter*, *Candidatus* Limnoluna, and *Sporichthyaceae*, were predicted to contribute to total enzymatic activities only during the first half of the experiment. Of these, *Sporichthyaceae* (Actinobacteria) has been associated with a free-living lifestyle (Bashenkhaeva et al. 2020). By contrast, *Cryomorphaceae* (Bacteroidia) and *Mycobacterium* (Actinobacteria) have been associated with a particle-attached lifestyle (Allgaier et al. 2007, Delmont et al. 2014, Reintjes et al. 2023), and from these, contribution of *Mycobacterium* to the community-wide predicted LAPase activity was observed only at the end of the experiment. It has been indicated that bacteria with a generalist lifestyle in terms of their habitat choice could shift between these two fractions depending on e.g. nutrient availability (Villalba et al. 2022) or changes in available substrates (Grossart 2010), but to our knowledge no detailed taxonomic studies on this topic exist yet.

Regarding export fluxes, OM quality is considered an important characteristic for microbial uptake and metabolism (Boyd and Trull 2007). The observed POC:PON ratio was above the Redfield ratio throughout the entire experiment (Fig. 2J), consequently the contribution of detritus consisting of mainly nonliving OM to total biovolume was relatively high (Supplementary Fig. S1B). Regardless, in the NC-treatment during the last three samplings of the experiment, LAPase and AGase shifted from being predominantly associated with free-living bacteria to the >3 µm fraction. APase activity showed a similar change, probably attributable to carbon acquisition, although the activity in 0.2–3 µm was not correlated with bacterial abundance. Additionally, BGase exhibited comparable activity between the 0.2–3 µm and >3 µm fractions. This indicates intense bacterial particle colonization and simultaneous succession of the bacterial community as a consequence of temporal changes in available substrates during the latter phase of the experiment. This would suggest attenuation of carbon flux to the seafloor if the colonized particles were small enough to stay suspended in the surface layer. Without direct measurements of sedimentation rates, we are unable to certainly address this as >3 µm fraction includes both suspended and sinking particles. Increasing particle bound LAPase activity toward the end of the experiment and the significant negative effect of NH_4^+ indicate nitrogen limitation of particle attached bacteria. Higher N

degradation relative to C also in the >3 µm size fraction implies that POM lost N faster compared to C thereby increasing the C:N ratio of potentially sinking material (Smith et al. 1992, Grossart and Ploug 2001).

Conclusions

Excess phosphate was not depleted during the experiment, and we found a relatively high potential of dissolved APase activity to play a substantial role in sustaining the surplus phosphate pool. These activities probably derived from microbial activity during low phosphate conditions prior to the experiment. In addition, grazing on heterotrophic bacteria probably also recycled phosphorus during the experiment and contributed to the excess phosphate pool. The computational approach predicting functional activities via 16S rRNA gene sequences suggested that taxa belonging to Actinobacteria and Alphaproteobacteria were potentially important producers of peptidolytic and glycolytic enzymes during the bacterioplankton bloom development when accessible substrates were still available at the beginning of the mesocosm experiment. Combined NC-amendment seemed to induce a shift toward particle-attached glycolytic, peptidolytic, and phosphomonoester degradation processes likely due to availability of settling surfaces for bacteria. Our findings indicate N- and C-limitation of heterotrophic bacteria with a faster degradation rate of peptides compared to polysaccharides, which implies a higher dissolution rate of N- compared to C-rich OM (Grossart and Ploug 2001). Measuring vertical patterns of EEA in the northern Baltic Sea could elucidate the potential of OM degradation in different layers of the water column, a necessary approach toward a better understanding of export fluxes and nutrient cycles. These studies should also include direct measurements of sedimentation rates and the composition of sinking OM.

Acknowledgments

We thank Joanna Norkko and Laura Kauppi for technical support, Jostein Solbakken and Göran Lundberg for assistance in setting up the mesocosms and Mervi Sjöblom, Jaana Koistinen, and Kia Rautava for inorganic and organic nutrient analyses at the Tvärminne Zoological Station. We thank Onni Talas foundation interns; Emma Forss, Neea Hanström, Anni Leinonen, and Marlena Grönqvist, for their help in the laboratory and field. We extend our thanks to Christiane Hassenrück for developing the bioinformatics tailored workflow partially used in this manuscript, her helpful suggestions, and valuable discussions regarding the metabolic prediction investigation. The study utilized the Finnish Environment Institute marine research infrastructure as a part of the national Finnish Marine Research Infrastructure (FINMARI) consortium.

Author contributions

Mari Vanharanta (Conceptualization, Data curation, Formal analysis, Funding acquisition, Investigation, Methodology, Visualization, Writing – original draft, Writing – review & editing), Mariano Santoro (Data curation, Formal analysis, Investigation, Methodology, Visualization, Writing – original draft, Writing – review & editing), Cristian Villena-Alemany (Investigation, Methodology, Writing – review & editing), Jonna Piiparinen (Formal analysis, Investigation, Methodology, Writing – review & editing), Kasia Piwosz (Formal analysis, Funding acquisition, Investigation, Methodology, Project administration, Writing – review & editing), Hans-Peter Grossart (Writing – review & editing), Matthias Labrenz (Writing – review & editing), and Kristian Spilling (Formal analysis, Funding acquisition, Methodology, Project administration, Supervision, Writing – review & editing)

Supplementary data

Supplementary data is available at *FEMSEC Journal* online.

Conflict of interest: The authors declare no conflict of interest.

Funding

This study was supported by the Transnational Access program of the EU H2020-INFRAIA project (number 731065) AQUACOSM—Network of Leading European AQUAtic MesoCOSM Facilities Connecting Mountains to Oceans from the Arctic to the Mediterranean—funded by the European Commission. Additional funding came from the Walter and Andrée de Nottbeck foundation (M.V. and K.S.), Koneen Säätiö (M.V.), Suomen Kulttuurirahasto (M.V.), Leibniz Science Campus Phosphorus Research Rostock in the funding line strategic networks of the Leibniz Association (M.S.), the National Science Centre, Poland under the Weave-UNISONO call in the Weave program (project number 2021/03/Y/NZ8/00076 to K.P.), and the German Science Foundation (DFG) (GR1540/37-1, Pycnotrap project to H.P.G.).

Data availability

Data from all measured parameters are available on PANGAEA (Vanharanta et al. 2024). The sequence data for this study have been deposited in the European Nucleotide Archive (ENA) at EMBL-EBI under accession number PRJEB72147 (https://www.ebi.ac.uk/ena/browser/view/PRJEB72147) via GFBio brokerage service (Diepenbroek et al. 2014).

References

Allers E, Gómez-Consarnau L, Pinhassi J *et al.* Response of *Alteromonadaceae* and *Rhodobacteriaceae* to glucose and phosphorus manipulation in marine mesocosms. *Environ Microbiol* 2007;**9**:2417–29.

Allgaier M, Bruckner S, Jaspers E *et al.* Intra- and inter-lake variability of free-living and particle-associated actinobacteria communities. *Environ Microbiol* 2007;**9**:2728–41.

Allison SD, Lu L, Kent AG *et al.* Extracellular enzyme production and cheating in *Pseudomonas fluorescens* depend on diffusion rates. *Front Microbiol* 2014;**5**. https://doi.org/10.3389/fmicb.2014.00169.

Azúa I, Unanue M, Ayo B *et al.* Influence of organic matter quality in the cleavage of polymers by marine bacterial communities. *J Plankton Res* 2003;**25**:1451–60.

Baltar F. Watch out for the "living dead": cell-free enzymes and their fate. *Front Microbiol* 2018;**8**.

Baltar F, Arístegui J, Gasol JM *et al.* High dissolved extracellular enzymatic activity in the deep central Atlantic Ocean. *Aquat Microb Ecol* 2010;**58**:287–302.

Baltar F, Legrand C, Pinhassi J. Cell-free extracellular enzymatic activity is linked to seasonal temperature changes: a case study in the Baltic Sea. *Biogeosciences* 2016;**13**:2815–21.

Baltar F, de Corte D, Yokokawa T. Bacterial stress and mortality may be a source of cell-free enzymatic activity in the marine environment. *Microbes Environ* 2019;**34**:83–8.

Barbera P. EPA-ng: efficient probabilistic assignment for DNA sequences. V.0.3.8. GitHub, 2019. https://github.com/pierrebarbera/epa-ng (1 March 2023, date last accessed).
Barbera P, Kozlov AM, Czech L *et al.* EPA-ng: massively parallel evolutionary placement of genetic sequences. *Syst Biol* 2019;**68**:365–9.
Bashenkhaeva MV, Galachyants YP, Khanaev IV *et al.* Comparative analysis of free-living and particle-associated bacterial communities of Lake Baikal during the ice-covered period. *J Great Lakes Res* 2020;**46**:508–18.
Bochdansky AB, Puskaric S, Herndl GJ. Influence of zooplankton grazing on free dissolved enzymes in the sea. *Mar Ecol Prog Ser* 1995;**121**:53–63.
Bochdansky AB, Clouse MA, Herndl GJ. Dragon kings of the deep sea: marine particles deviate markedly from the common number-size spectrum. *Sci Rep* 2016;**6**. https://doi.org/10.1038/srep22633.
Boyd P, Trull T. Understanding the export of biogenic particles in oceanic waters: is there consensus?. *Prog Oceanogr* 2007;**72**:276–312.
Bunse C, Bertos-Fortis M, Sassenhagen I *et al.* Spatio-temporal interdependence of bacteria and phytoplankton during a Baltic Sea spring bloom. *Front Microbiol* 2016;**7**. https://doi.org/10.3389/fmicb.2016.00517.
Bunse C, Israelsson S, Baltar F *et al.* High frequency multi-year variability in Baltic Sea microbial plankton stocks and activities. *Front Microbiol* 2019;**9**. https://doi.org/10.3389/fmicb.2018.03296.
Callahan BJ, McMurdie PJ, Rosen MJ *et al.* DADA2: high-resolution sample inference from Illumina amplicon data. *Nat Methods* 2016;**13**:581–3.
Camarena-Gómez MT, Ruiz-González C, Piiparinen J *et al.* Bacterioplankton dynamics driven by interannual and spatial variation indiatom and dinoflagellate spring bloom communities in the Baltic Sea. *Limnol Oceanogr* 2020;**66**:255–271.
Cho BC, Azam F. Major role of bacteria in biogeochemical fluxes in the ocean's interior. *Nature* 1988;**332**:441.
Chróst RJ. Environmental control of the synthesis and activity of aquatic microbial ectoenzymes. In: Chróst R.J. (ed.), *Microbial Enzymes in Aquatic Environments*. Brock/Springer Series in Contemporary Bioscience. New York: Springer, 1991.
Chrzanowski TH, Kyle M. Ratios of carbon, nitrogen and phosphorus in *Pseudomonas fluorescens* as a model for bacterial element ratios and nutrient regeneration. *Aquat Microb Ecol* 1996;**10**:115–22.
Delmont TO, Hammar KM, Ducklow HW *et al. Phaeocystis antarctica* blooms strongly influence bacterial community structures in the Amundsen Sea polynya. *Front Microbiol* 2014;**5**. https://doi.org/10.3389/fmicb.2014.00646.
Diepenbroek M, Glöckner F, Grobe P *et al.* Towards an integrated biodiversity and ecological research data management and archiving platform: the German Federation for the Curation of Biological Data (GFBio). In: Plödereder E, Grunske L, Schneider E, Ull D (eds.), *Proceedings of the Informatik 2014–Big Data Komplexität Meistern*. GI-edn. Vol. **232**. Lecture Notes in Informatics (LNI). Bonn: Köllen Verlag; 2014, 1711–24.
Douglas GM, Maffei VJ, Zaneveld JR *et al.* PICRUSt2 for prediction of metagenome functions. *Nat Biotechnol* 2020;**38**:685–8.
Eigemann F, Rahav E, Grossart H-P *et al.* Phytoplankton producer species and transformation of released compounds over time define bacterial communities following phytoplankton dissolved organic matter pulses. *Appl Environ Microbiol* 2023;**89**:1–16.
Eilola K, Stigebrandt A. On the seasonal nitrogen dynamics of the Baltic proper biochemical reactor. *J Mar Res* 1999;**57**:693–713.
Fawcett SE, Ward BB. Phytoplankton succession and nitrogen utilization during the development of an upwelling bloom. *Mar Ecol Prog Ser* 2011;**428**:13–31.
Fuhrman J, Azam F. Thymidine incorporation as a measure of heterotrophic bacterioplankton production in marine surface waters: evaluation and field results. *Mar Biol* 1982;**66**:109–20.
Gasol JM, Del Giorgio PA. Using flow cytometry for counting natural planktonic bacteria and understanding the structure of planktonic bacterial communities. *Sci Mar* 2000;**64**:197–224.
González-Gil S, Keafer BA, Jovine RV *et al.* Detection and quantification of alkaline phosphatase in single cells of phosphorus-starved marine phytoplankton. *Mar Ecol Prog Ser* 1998;**164**:21–35.
Grasshoff K, Ehrhardt M, Kremling K. *Methods of Seawater Analysis*. 3rd edn. Weinheim: Wiley-VCH, 1999.
Grossart H-P. Ecological consequences of bacterioplankton lifestyles: changes in concepts are needed. *Environ Microbiol Rep* 2010;**2**:706–14.
Grossart H-P, Ploug H. Microbial degradation of organic carbon and nitrogen on diatom aggregates. *Limnol Oceanogr* 2001;**46**:267–77.
Grossart H-P, Simon M. Bacterial colonization and microbial decomposition of limnetic organic aggregates (lake snow). *Aquat Microb Ecol* 1998;**15**:127–40.
Grossart H-P, Hietanen S, Ploug H. Microbial dynamics on diatom aggregates in Øresund, Denmark. *Mar Ecol Prog Ser* 2003;**249**:69–78.
Grossart H-P, Engel A, Arnosti C *et al.* Microbial dynamics in autotrophic and heterotrophic seawater mesocosms. III. Organic matter fluxes. *Aquat Microb Ecol* 2007a;**49**:143–56.
Grossart H-P, Tang KW, Kiørboe T *et al.* Comparison of cell-specific activity between free-living and attached bacteria using isolates and natural assemblages. *FEMS Microbiol Lett* 2007b;**266**:194–200.
Grossart H-P, Van den Wyngaert S, Kagami M *et al.* Fungi in aquatic ecosystems. *Nat Rev Microbiol* 2019;**17**:339–54.
Hansell DA. Recalcitrant dissolved organic carbon fractions. *Annu Rev Mar Sci* 2013;**5**:421–45.
Heiskanen AS. Factors governing sedimentation and pelagic nutrient cycles in the northern Baltic Sea. *Monogr Boreal Env Res* 1998;**8**:1–80.
HELCOM 2008 Helsinki Commission (HELCOM). 2008. Programme for monitoring of eutrophication and its effects. Annex C-11 guidelines concerning bacterioplankton growth determination. In: *Manual for Marine Monitoring in the COMBINE Programme of HELCOM. Annex C-1 :* 9. Helsinki: HELCOM.
Heldal M, Norland S, Fagerbakke KM *et al.* The elemental composition of bacteria: a signature of growth conditions?. *Mar Pollut Bull* 1996;**33**:3–9.
Hoppe HG. Significance of exoenzymatic activities in the ecology of brackish water: measurements by means of methylumbelliferyl-substrates. *Mar Ecol Prog Ser* 1983;**11**:299–308.
Hoppe HG. Microbial extracellular enzyme activity: a new key parameter in aquatic ecology. In: Chróst RJ (ed.), *Microbial Enzymes in Aquatic Environments. Brock/Springer Series in Contemporary Bioscience*. New York: Springer, 1991.
Hoppe HG. Phosphatase activity in the sea. *Hydrobiology* 2003;**493**:187–200.
Hugerth LW, Larsson J, Alneberg J *et al.* Metagenome-assembled genomes uncover a global brackish microbiome. *Genome Biol* 2015;**16**:1–18.
Inkscape Project. Inkscape. Version 1.3.1. 2020. https://inkscape.org/ (23 October 2023, date last accessed).
Ivančić I, Pfannkuchen M, Godrijan J *et al.* Alkaline phosphatase activity related to phosphorus stress of microphytoplankton in different trophic conditions. *Prog Oceanogr* 2016;**146**:175–86.
Jespersen AM, Christoffersen K. Measurements of chlorophyll a from phytoplankton using ethanol as extraction solvent. *Arch Hydrobiol* 1987;**109**:445–54.

Karner M, Herndl GJ. Extracellular enzymatic activity and secondary production in free-living and marine-snow-associated bacteria. *Mar Biol* 1992;**113**:341–7.

Karner M, Rassoulzadegan F. Extracellular enzyme activity: indications for high short-term variability in a coastal marine ecosystem. *Microb Ecol* 1995;**30**:143–56.

Kirchman DL, K´nees E, Hodson RE. Leucine incorporation and its potential as a measure of protein synthesis by bacteria in natural systems. *Appl Environ Microb* 1985;**49**:599–607.

Kirchman DL. The uptake of inorganic nutrients by heterotrophic bacteria. *Microb Ecol* 1994;**28**:255–71.

Kirchman DL. The ecology of *Cytophaga–Flavobacteria* in aquatic environments. *FEMS Microbiol Ecol* 2002;**39**:91–100.

Klindworth A, Pruesse E, Schweer T *et al.* Evaluation of general 16S ribosomal RNA gene PCR primers for classical and next-generation sequencing-based diversity studies. *Nucleic Acids Res* 2013;**41**:e1.

Koch MS, Kletou DC, Tursi R. Alkaline phosphatase activity of water column fractions and seagrass in a tropical carbonate estuary, Florida Bay. *Estuar Coast Shelf Sci* 2009;**83**:403–13.

Koistinen J, Sjöblom M, Spilling K. Determining inorganic and organic phosphorus. In: Spilling K (ed.), *Biofuels from Algae*. New York: Human Press, 2017, 87–94.

Köster J, Rahmann S. Snakemake—a scalable bioinformatics workflow engine. *Bioinformatics* 2012;**28**:2520–2.

Lapébie P, Lombard V, Drula E *et al.* Bacteroidetes use thousands of enzyme combinations to break down glycans. *Nat Commun* 2019;**10**:2043.

Length R. emmeans: estimated Marginal Means, aka Least-squares Means. R package version 1.9.0. CRAN, 2023. https://CRAN.R-project.org/package=emmeans.

Lignell R, Hoikkala L, Lahtinen T. Effects of inorganic nutrients, glucose and solar radiation on bacterial growth and exploitation of dissolved organic carbon and nitrogen in the northern Baltic Sea. *Aquat Microb Ecol* 2008;**51**:209–221.

Lilover M-J, Stips A. The variability of parameters controlling the cyanobacteria bloom biomass in the Baltic Sea. *J Mar Syst* 2008;**74**:S108–15.

Lips I, Lips U. The importance of *mesodinium rubrum* at post-spring bloom nutrient and phytoplankton dynamics in the vertically stratified Baltic Sea. *Front Mar Sci* 2017;**4**. https://doi.org/10.3389/fmars.2017.00407.

Luo H, Benner R, Long RA *et al.* Subcellular localization of marine bacterial alkaline phosphatases. *Proc Natl Acad Sci* 2009;**106**:21219–23.

Lyons MM, Dobbs FC. Differential utilization of carbon substrates by aggregate-associated and water-associated heterotrophic bacterial communities. *Hydrobiologia* 2012;**686**:181–193.

Mahaffey C, Reynolds S, Davis CE *et al.* Alkaline phosphatase activity in the subtropical ocean: insights from nutrient, dust and trace metal addition experiments. *Front Mar Sci* 2014;**1**. https://doi.org/10.3389/fmars.2014.00073.

Malfatti F, Turk V, Tinta T *et al.* Microbial mechanisms coupling carbon and phosphorus cycles in phosphorus-limited northern Adriatic Sea. *Sci Total Environ* 2014;**470–471**:1173–83.

Middelboe M, Sondergaard M, Letarte Y *et al.* Attached and free-living bacteria: production and polymer hydrolysis during a diatom bloom. *Microb Ecol* 1995;**29**:231–48.

Mohit V, Archambault P, Toupoint N *et al.* Phylogenetic differences in attached and free-living bacterial communities in a temperate coastal lagoon during summer, revealed via high-throughput 16S rRNA gene sequencing. *Appl Environ Microbiol* 2014;**80**:2071–83.

Murray AE, Arnosti C, De La Rocha CL *et al.* Microbial dynamics in autotrophic and heterotrophic seawater mesocosms. II. Bacterioplankton community structure and hydrolytic enzyme activities. *Aquat Microb Ecol* 2007;**49**:123–41.

Nausch M. Alkaline phosphatase activities and the relationship to inorganic phosphate in the Pomeranian Bight (southern Baltic Sea). *Aquat Microb Ecol* 1998;**16**:87–94.

Nausch M. Experimental evidence for interactions between bacterial peptidase and alkaline phosphatase activity in the Baltic Sea. *Aquat Ecol* 2000;**34**:331–43.

Nausch M, Nausch G. Bacterial utilisation of phosphorus pools after nitrogen and carbon amendment and its relation to alkaline phosphatase activity. *Aquat Microb Ecol* 2004;**37**:237–45.

Nausch M, Pollehne F, Kerstan E. Extracellular enzyme activities in relation to hydrodynamics in the Pomeranian Bight (southern Baltic Sea). *Microb Ecol* 1998;**36**:251–8.

Nausch M, Achterberg EP, Bach LT *et al.* Concentrations and uptake of dissolved organic phosphorus compounds in the Baltic Sea. *Front Mar Sci* 2018;**5**:386.

Nercessian O, Noyes E, Kalyuzhnaya MG *et al.* Bacterial populations active in metabolism of C1 compounds in the sediment of Lake Washington, a freshwater lake. *Appl Environ Microbiol* 2005;**71**:6885–99.

Niemi Å. Blue-green algal blooms and N:P ratio in the Baltic Sea. *Acta Botanica Fennica* 1979;**110**:57–61.

Norland S. The relationship between biomass and volume of bacteria. In: Kemp PF, Cole JJ, Sherr BF, Sherr EB (eds.), *Handbook of Methods in Aquatic Microbial Ecology*. Boca Raton: CRC Press, 1993, 303–7.

Pinheiro J, Bates D, R Core Team. nlme: linear and nonlinear mixed effects models_. R package version 3.1-162. CRAN, 2023. https://CRAN.R-project.org/package=nlme.

Piwosz K, Salcher MM, Zeder M *et al.* Seasonal dynamics and activity of typical freshwater bacteria in brackish waters of the Gulf of Gdańsk. *Limnol Oceanogr* 2013;**58**:817–26.

Ploug H, Grossart H-P. Bacterial growth and grazing on diatom aggregates: respiratory carbon turnover as a function of aggregate size and sinking velocity. *Limnol Oceanogr* 2000;**45**:1467–75.

R Core Team. *R: A Language and Environment for Statistical Computing*. Vienna: R Foundation for Statistical Computing, 2022.

Raateoja M, Kuosa H, Hällfors S. Fate of excess phosphorus in the Baltic Sea: a real driving force for cyanobacterial blooms?. *J Sea Res* 2011;**65**:315–21.

Rahm L, Jönsson A, Wulff F. Nitrogen fixation in the Baltic proper: an empirical study. *J Mar Syst* 2000;**25**:239–48.

Ramin KI, Allison SD. Bacterial tradeoffs in growth rate and extracellular enzymes. *Front Microbiol* 2019;**10**. https://doi.org/10.3389/fmicb.2019.02956.

Redfield AC. The biological control of chemical factors in the environment. *Am Sci* 1958;**64**:205–21.

Reintjes G, Heins A, Wang C *et al.* Abundance and composition of particles and their attached microbiomes along an Atlantic Meridional Transect. *Front Mar Sci* 2023;**10**. https://doi.org/10.3389/fmars.2023.1051510.

Rengefors K, Pettersson K, Blenckner T *et al.* Species-specific alkaline phosphatase activity in freshwater spring phytoplankton: application of a novel method. *J Plankton Res* 2001;**23**:435–43.

Rieck A, Herlemann DPR, Jürgens K *et al.* Particle-associated differ from free-living bacteria in surface waters of the Baltic Sea. *Front Microbiol* 2015;**6**. https://doi.org/10.3389/fmicb.2015.01297.

Salazar-Alekseyeva K, Herndl GJ, Baltar F. Release of cell-free enzymes by marine pelagic fungal strains. *Front Fungal Biol* **4**;2023. https://doi.org/10.3389/ffunb.2023.1209265.

Salerno M, Stoecker DK. Ectocellular glucosidase and peptidase activity of the mixotrophic dinoflagellate *Prorocentrum minimum* (Dinophyceae). *J Phycol* 2009;**45**:34–45.

Salonen K. A versatile method for the rapid and accurate determination of carbon by high temperature combustion. *Limnol Oceanogr* 1979;**24**:177–83.

Sharp JH, Peltzer ET, Alperin MJ *et al.* Measurement of dissolved organic carbon and nitrogen in natural waters: procedures subgroup report. *Mar Chem* 1993;**41**:37–49.

Sherr BF, Sherr EB, Fallon RD. Use of monodispersed, fluorescently labeled bacteria to estimate in situ protozoan bacterivory. *Appl Environ Microbiol* 1987;**53**:958–65.

Simon M, Azam F. Protein content and protein synthesis rates of planktonic marine bacteria. *Mar Ecol Prog Ser* 1989;**51**:201–13.

Simon M, Grossart H-P, Schweitzer B *et al.* Microbial ecology of organic aggregates in aquatic ecosystems. *Aquat Microb Ecol* 2002;**28**:175–211.

Smith DC, Azam F. A simple, economical method for measuring bacterial protein synthesis rates in seawater using 3H-leucine. *Mar Microb Food Webs* 1992;**6**:107–14.

Smith DC, Simon M, Alldredge AL *et al.* Intense hydrolytic enzyme activity on marine aggregates and implication for rapid particle dissolution. *Nature* 1992;**359**:139–41.

Solórzano L, Sharp JH. Determination of total dissolved phosphorus and particulate phosphorus in natural waters. *Limnol Oceanogr* 1980;**25**:754–8.

Spilling K, Olli K, Lehtoranta J *et al.* Shifting diatom–dinoflagellate dominance during spring bloom in the Baltic Sea and its potential effects on biogeochemical cycling. *Front Mar Sci* 2018;**5**. https://doi.org/10.3389/fmars.2018.00327.

Spilling K, Piiparinen J, Achterberg EP *et al.* Extracellular enzyme activity in the coastal upwelling system off Peru: a mesocosm experiment. *Biogeosciences* 2023;**20**:1605–19.

Spilling K, Vanharanta M, Santoro M *et al.* Effects of excess phosphate on a coastal plankton community. *Biorxiv* 2024. https://doi.org/10.1101/2024.02.05.576994.

Steen AD, Arnosti C. Long lifetimes of β-glucosidase, leucine aminopeptidase, and phosphatase in Arctic seawater. *Mar Chem* 2011;**123**:127–32.

Steinberg DK, van Mooy BAS, Buesseler KO *et al.* Bacterial vs. zooplankton control of sinking particle flux in the ocean's twilight zone. *Limnol Oceanogr* 2008;**253**:1327–38.

Strojsová E, Vrba J, Nedoma J *et al.* Seasonal study of extracellular phosphatase expression in the phytoplankton of a eutrophic reservoir. *Eur J Phycol* 2003;**38**:295–306.

Tada Y, Grossart H-P. Community shifts of actively growing lake bacteria after N-acetyl-glucosamine addition: improving the BrdU-FACS method. *ISME J* 2014;**8**:441–54.

Tamelander T, Heiskanen AS. Effects of spring bloom phytoplankton dynamics and hydrography on the composition of settling material in the coastal northern Baltic Sea. *J Mar Syst* 2004;**52**:217–34.

Thingstad TF, Bellerby RGJ, Bratbak G *et al.* Counterintuitive carbon-to-nutrient coupling in an Arctic pelagic ecosystem. *Nature* 2008;**455**:387–90.

Thomson B, Wenley J, Currie K *et al.* Resolving the paradox: continuous cell-free alkaline phosphatase activity despite high phosphate concentrations. *Mar Chem* 2019;**214**:103671.

Traving SJ, Balmonte JP, Seale D *et al.* On single-cell enzyme assays in marine microbial ecology and biogeochemistry. *Front Mar Sci Sec Aquat Microbiol* 2022;**9**. https://doi.org/10.3389/fmars.2022.846656.

Traving SJ, Thygesen UH, Riemann L *et al.* A model of extracellular enzymes in free-living microbes: which strategy pays off?. *Appl Environ Microb* 2015;**81**:7385–93.

Vadstein O, Olsen LM, Busch A *et al.* Is phosphorus limitation of planktonic heterotrophic bacteria and accumulation of degradable DOC a normal phenomenon in phosphorus-limited systems? A microcosm study. *FEMS Microbiol Ecol* 2003;**46**:307–16.

Vahtera E, Conley DJ, Gustafsson BG *et al.* Internal ecosystem feedback enhance nitrogen-fixing cyanobacteria blooms and complicate management in the Baltic Sea. *Ambio* 2007;**36**:186–94.

Vanharanta M, Spilling K. The uptake of excess phosphate at low inorganic N:P ratio in a coastal sea afflicted with eutrophication. *Mar Ecol Prog Ser* 2023;**718**:23–37.

Vanharanta M, Santoro M, Villena-Alemany C *et al.* Effect of decreasing inorganic N:P ratio on the plankton community—INN:PP. PANGAEA. 2024. https://doi.org/10.1594/PANGAEA.966040.

Villalba LA, Karnatak R, Grossart H-P *et al.* Flexible habitat choice of pelagic bacteria increases system stability and energy flow through the microbial loop. *Limnol Oceanogr* 2022;**67**:1402–15.

Villena-Alemany C, Mujakić I, Fecskeová LK *et al.* Phenology and ecological role of aerobic anoxygenic phototrophs in freshwaters. *Microbiome* 2024;**12**:65.

Wickham H. *GGplot2: Elegant Graphics for Data Analysis*. New York: Springer, 2016.

Ylla I, Romaní AM, Sabater S. Labile and recalcitrant organic matter utilization by river biofilm under increasing water temperature. *Microb Ecol* 2012;**64**:593–604.

Zhao L, Brugel S, Ramasamy KP *et al.* Bacterial community responses to planktonic and terrestrial substrates in coastal northern Baltic Sea. *Front Mar Sci* 2023;**10**. https://doi.org/10.3389/fmars.2023.1130855.

Ziervogel K, Arnosti C. Polysaccharide hydrolysis in aggregates and free enzyme activity in aggregate-free seawater from the northeastern Gulf of Mexico. *Environ Microbiol* 2008;**10**:289–99.

Ziervogel K, Steen AD, Arnosti C. Changes in the spectrum and rates of extracellular enzyme activities in seawater following aggregate formation. *Biogeosciences* 2010;**7**:1007–15.

Received 7 February 2024; **revised** 10 June 2024; **accepted** 19 July 2024